Specific cell states underlie complex tissue regeneration in spiny mice

Emilio Oviedo Rivadeneira[1], Robyn Allen[1], Mike Adam[2], and Ashley W. Seifert[1,3,4*]

[1]*Department of Biology, University of Kentucky, Lexington, KY 40506, USA*
[2]*Division of Experimental Hematology and Cancer Biology, Cancer and Blood Diseases Institute, Cincinnati Children's Hospital Medical Center, Cincinnati, OH, USA*
[3]*Department of Veterinary Anatomy and Physiology, University of Nairobi, Nairobi, Kenya*
[4]*Aligning Science Across Parkinson's (ASAP) Collaborative Research Network, Chevy Chase, MD 20815, USA*

ORCID: Ashley W. Seifert, 0000-0001-6576-3664

Key words: Cell proliferation, regeneration, cell cycle, cell state, fibroblasts, chondroblasts

*To whom correspondence should be addressed: Ashley W. Seifert, e-mail: awseifert@uky.edu

SUMMARY STATEMENT

Comparing regenerative vs. fibrotic healing, we identify injury-induced cell states associated with persistent cell cycle progression and complex tissue regeneration in mammals.

ABSTRACT

Cell proliferation is an elemental feature of epimorphic regeneration in vertebrate taxa. We previously reported that in contrast to fibrotic repair observed in laboratory mouse (*Mus*) strains, highly regenerative spiny mice (*Acomys* spp.) exhibit cell cycle progression and cell proliferation to faithfully replace missing tissue. However, little is known about proliferation dynamics, and specific cell types and states that may contribute to complex tissue regeneration in mammals. Using temporal pulse-chase experiments, we show that stromal cells in *Acomys dimidiatus* rapidly re-enter the cell cycle in response to injury and maintain tight spatiotemporal control of cell cycle progression to restrict the proliferative population to a distal area relative to the injury. Conversely, *Mus* stromal cells incorporate thymidine analogs without cell division supporting an S-phase arrest after D10. Deploying immunostaining and scRNA-seq, we identify several key cell types (CRABP1+, αSMA+) differentially associated with regenerating versus scar tissue. Importantly, our single cell data revealed distinct gene expression profiles for cross-species stromal cell types, identifying cell states specific for regenerative or fibrotic healing. While CRABP1+ fibroblasts are enriched in *Acomys* ears before and after injury, similar fibroblasts enriched in young, postnatal *Mus* ears remain unable to promote regeneration. Our data underscore the finely regulated dynamics of proliferating cells during regeneration and emphasize that regeneration depends on multiple factors including the presence of specific cell types and the ability of cells to acquire specific states.

68 **Key Conclusions:**

69 -Differentiated cells in *Acomys*, *Mus* and *Danio* re-enter the cell cycle in response to injury,
70 while homeostatic cycling cells contribute to blastema formation in *Ambystoma*

71 -Pulse-chase thymidine analog labeling shows tight spatiotemporal control of proliferating
72 stromal cells during regeneration in *Acomys*.

73 -Following injury, CRABP1 and αSMA are expressed in distinct stromal cell populations in
74 *Acomys* but are co-expressed in *Mus* stromal cell populations.

75 -Species-specific cell states underlie regenerative and fibrotic repair

76 -CRABP1+ cells are lost during embryonic development in *Mus* ear pinna but are retained in
77 *Acomys* to adulthood.

78 -Young neonatal *Mus* with abundant CRABP1+ cells still fail to execute regenerative healing

79

80

INTRODUCTION

Epimorphic regeneration is mediated by the accumulation of local progenitor cells that proliferate to form a blastema and subsequently differentiate to replace missing or damaged tissue (Morgan, 1901). With few exceptions (e.g. hydra, colonial animals, etc.), most regeneration-competent invertebrate and vertebrate species use epimorphic regeneration to rebuild missing tissue. Seminal studies using urodeles, zebrafish, and planarians explored the dynamics of proliferating cells to understand their origin, proliferative rates, migration patterns, and responses to different injury types (Hays & Fischman, 1961; Poleo et al., 2001; Wallace, 1981; Wenemoser & Reddien, 2010). For example, thymidine analogs applied to amputated newt limbs revealed that cells start to synthesize DNA in tissues adjacent to the wound site (e.g. muscle, connective tissue, periosteum, etc.) and that these proliferating cells are then liberated and maintained distally from the injury in the blastema (Hays & Fischman, 1961). Similar studies in axolotls investigated cell cycle length, factors required to maintain proliferation and the impact of inhibiting proliferation on regeneration (Maden & Wallace, 1976; Wallace, 1981; Wallace & Maden, 1976). Different types of injury trigger distinct mitotic responses in planarians. An amputation, for example, can cause both local and systemic responses, while any other injury that does not remove tissue triggers only the first systemic response without triggering a local one (Wenemoser & Reddien, 2010). Similarly, studies in zebrafish have improved our understanding of the spatiotemporal distribution of proliferating cells in the blastema (Nechiporuk & Keating, 2002; Poleo et al., 2001). All these studies have advanced our understanding of the dynamics of the proliferative population in highly regenerative animals. However, the spatiotemporal dynamics of proliferating cells in regenerative mammals remains poorly understood.

Complex tissue regeneration in vertebrates has been primarily studied in fishes, amphibians and invertebrates. However, some mammals exhibit bona fide regeneration (Billingham et al., 1959; Borgens, 1982; Carlson, 2005; Gawriluk et al., 2016; Goss & Grimes, 1972; Neeham, 1953; Seifert et al., 2012; Vorontsova et al., 1960). For instance, patterned musculoskeletal tissue is reconstituted after removal with a full thickness hole punch through the ear pinna in some lagomorphs and deomyine rodents (e.g., *Acomys* and *Lophuromys*) (Gawriluk et al., 2016; Goss, 1980; Goss & Grimes, 1972; Seifert et al., 2012). Comparative studies

112 between regenerative and non-regenerative rodents showed that spiny mice (*Acomys*) can
113 regenerate ear pinna tissue after full thickness excisional injury; a response mediated by cell
114 proliferation and blastema formation. In response to an identical injury, however, laboratory
115 mice (*Mus*) cannot regenerate missing tissue and while cells are activated to re-enter the cell
116 cycle in response to injury, these cells are arrested shortly afterwards (Gawriluk et al., 2016;
117 Seifert et al., 2012).
118 Generally speaking, complex tissue cell proliferation in non-regenerative mammals
119 occurs exclusively during embryonic development, while cell cycle progression and cell division
120 become increasingly restricted to stem and progenitor cells in tissues that require constant
121 turnover during postembryonic development and adulthood (Cheung & Rando, 2013; Liu et al.,
122 2019; Orford & Scadden, 2008). This raises a question about the identity of cells capable of
123 maintaining cell cycle progression in regenerative mammals. Said another way, are there specific
124 cell types or cell states needed for regeneration to occur? In highly regenerative vertebrates,
125 multiple studies have pinpointed that blastema formation is supported by cellular re-
126 programming (termed dedifferentiation by most investigators) of lineage-restricted progenitors
127 located near the wound site (Echeverri et al., 2001; Gerber et al., 2018; Jopling et al., 2010;
128 Leigh et al., 2018). Interestingly, while lineage-restricted progenitors have been shown to
129 support digit tip regeneration in *Mus* (G. L. Johnson et al., 2020; Lehoczky et al., 2011;
130 Rinkevich et al., 2011), subsequent research showed that progenitor cell activation is important
131 but also the capacity of mesenchymal cells to maintain a specific transcriptomic state associated
132 with regeneration (Storer et al., 2020). Similar observations come from research investigating
133 deer antler velvet regeneration. Research comparing injured velvet versus dorsal back skin found
134 that while both skin types have *Acta2*+ myofibroblast cells, specific transcriptomic profiles were
135 associated with location. Importantly, this work showed that all velvet skin fibroblasts can access
136 regenerative regulatory networks that skew them to an immunosuppressive, pro-regenerative
137 fetal phenotype, while back skin fibroblasts express genes related to an inflammatory, pro-
138 fibrotic healing outcome (Sinha et al., 2022). Other wound healing studies, suggest that large
139 skin wounds capable of pro-regenerative healing are biased to use a specific fibroblast subtype
140 that is inhibited in fibrotic responses; a finding that is also associated with better healing
141 outcomes in neonatal *Mus* and human skin (Guerrero-Juarez et al., 2019; Mine et al., 2008; Phan

142 et al., 2021a). Together, these studies support that access to regenerative cell states ***and*** the
143 presence of specific cell types is essential to promote a regenerative outcome.
144 Here we use the spiny mouse ear pinna regeneration model to explore controlled cell
145 proliferation in adult mammals. Leveraging a comparative approach to fibrotic repair in
146 laboratory mice, we explore the spatiotemporal dynamics of proliferating cells and begin to
147 identify cell types that participate in regeneration. First, we use a pulse-chase method to quantify
148 cell cycle activation in regenerative vertebrates with determinate and indeterminate growth and
149 find that growth mode is not strictly associated with regenerative ability or the lack thereof.
150 Additionally, this analysis found no evidence of long-range cell activation in response to injury.
151 Using a pulse-chase labeling strategy, we show that proliferating cells maintain a distal position
152 relative to the wound site, while cells in the proximal compartment exit the cell cycle and
153 differentiate. Finally, using a combination of immunostaining and scRNA-sequencing, we
154 identify similar cell types across species that express distinct transcriptomic states associated
155 with regenerative or fibrotic repair supporting that species-specific cell states underlie
156 regeneration and scaring.
157
158 **METHODS**
159
160 **Animal care**. Sexually mature, spiny mice (*Acomys dimidiatus* - aged six months to one year
161 old) and *Mus musculus*, ~three months old) were obtained from our in-house breeding colonies
162 at the University of Kentucky. Animals were maintained on a 12:12 h L:D light cycle. Both
163 species were fed 14% mouse chow (Teklad Global 2014, Harlan Laboratories) and *Acomys* diets
164 were supplemented with black sunflower seeds. All animal experiments were approved by
165 University of Kentucky Institutional Animal Care and Use Committee (IACUC) under protocol
166 2013–3254.
167
168 **4mm ear punch assay regeneration assay**. A 4mm full thickness excisional punch through the
169 ear pinna serves as a tissue regeneration assay (Gawriluk et al., 2016). Animals were
170 anesthetized with 3% vaporized isoflurane (v/v) (Henry Schein Animal Health, Dublin, OH) at 1
171 psi oxygen flow rate. A 4mm biopsy punch (Sklar Instruments, West Chester, PA) was used to
172 create a through-and-through hole in the right and left ear pinna. Ear tissue was collected at

173 specified time points using an 8mm biopsy punch (Sklar Instruments, West Chester, PA)
174 circumscribing the original injury. The published protocol can be found here:
175 dx.doi.org/10.17504/protocols.io.bp2l6dx65vqe/v1.
176
177 **Pulse-chase experiments**. We injected Ethynyl deoxyuridine (EdU) (10 ug/g) and
178 Bromodeoxyuridine (BrdU) (1 ug/g) diluted in normal saline, for pulse-chase experiments to
179 label and track cycling cells (the published protocol can be found here:
180 dx.doi.org/10.17504/protocols.io.261gerdmol47/v1). Both solutions were injected
181 intraperitoneally with a difference of five days between the EdU and BrdU injections. EdU and
182 BrdU injections were given as three separate injections, one every three hours over a period of
183 nine hours. The left ear pinna was collected after the EdU pulse to assess baseline cell numbers
184 in S-phase, and the right pinna was collected after the BrdU pulse to track single (EdU+ or
185 BrdU+) and double positive cells. The injection scheme was as follows: the first group of
186 animals was injected with EdU at D0 and BrdU at D5, the next group was injected with EdU at
187 D5 and BrdU at D10 and so on until D30. Hence, tissue samples were collected at 0, 5, 10, 15,
188 20, 25, and 30-days post injury.
189 Our experimental scheme allowed us to distinguish cells that (i) were in S-phase at the
190 time of the EdU injections and stopped proliferating within next five days (Edu+ alone); (ii) were
191 in S-phase at the time of the EdU injections, divided multiple times over five days diluting the
192 EdU, and remained in the cell cycle acquiring BrdU (weak EdU+/ strong BrdU+) - because each
193 cell division dilutes the EdU by half, a scenario where EdU is not detectable is possible, and
194 these cells would contribute to the BrdU+ alone counts); (iii) cells not in S-phase during the EdU
195 pulse but were cycling during the BrdU injections (BrdU+ alone); (iv) cells that acquired EdU,
196 divided only a few times, and remained in the cell cycle during the BrdU chase (strong EdU+/
197 strong Brdu+).
198
199 **Histology, EdU detection and Immunohistochemistry**. Harvested tissue was fixed
200 overnight in 10% neutral buffered formalin (NBF) (Thermo Fisher Scientific Inc. Epredia
201 5701) at 4˚C on a shaker. After 16-20 hrs the tissue was washed 3x with PBS, 3 minutes
202 per wash, followed by 3x 70% ethanol washes for dehydration and storage at 4˚C. Stored
203 tissue was processed for paraffin (Leica Biosystems, Buffalo Grove, IL, Formula "R"

204 REF: 3801450) embedding using a Histo5 tissue processor machine (Milestone). Samples
205 were sectioned at 5µm. EdU was detected using click chemistry as follows: Tissue
206 sections were de-paraffinized and rehydrated. Antigen retrieval was performed if co-
207 stained with antibodies. Tissues were washed two times for 10 minutes in Tris-buffered
208 saline (TBS) to incubate in the prepared reaction cocktail (see table below) for 30
209 minutes at RT protected from light. Tissues were washed two times in TBS for 5 minutes
210 and if co-stained with antibodies were blocked following the fluorescent IHC protocol for
211 BrdU and cell type specific antibodies tissue sections were deparaffinized and re-
212 hydrated. Tissues were then exposed to high heat antigen retrieval in a steamer in antigen
213 unmasking TRIS or citric acid-based solutions (Vector Laboratories, Inc.). After a 5-
214 minute wash, tissues were blocked in blocking serum (see table below) for 30 minutes at
215 RT. Tissues were then incubated with primary antibody diluted in blocking serum at 4 ˚C
216 overnight. After a 5 minutes wash, tissues were incubated in secondary antibody diluted
217 in blocking serum for 30 min at RT. Tissue samples were incubated with Hoechst 33342
218 for 5 minutes at RT and then dried and mounted in Prolong. Finally, protein similarity
219 was compared to assess antibody binding efficacy (Supplementary table S1). For
220 complete protocol details regarding paraffin sections
221 (dx.doi.org/10.17504/protocols.io.6qpvr9353vmk/v1), immunohistochemistry
222 (dx.doi.org/10.17504/protocols.io.n92ldrmd8g5b/v1), and EdU detection on sections
223 (dx.doi.org/10.17504/protocols.io.e6nvwbdrzvmk/v1).
224

EdU reaction cocktail	
Components	**Volume (ul)**
2 M Tris, pH 8.5	5
50 mM CuSO4	2
0.5 M ascorbic acid	20
Alexa fluor azide (0.25 mg/ml)	0.2
ddH2O	73
Total	100

225

Primary Antibodies					
Antibody	**Company, Cat#**	**RRID**	**Host species**	**Dilution**	**Antigen retrieval**
Anti-BrdU (Bromodeoxyuridine)	Abcam, Ab6326	AB_305426	Rat	1:500	Citric Acid

Anti-wide spectrum Cytokeratin	Abcam, Ab9377	AB_307222	Rabbit	1:500	None
Anti-ionized calcium-binding adapter molecule 1 (IBA1)	Novus Biologicals, NB100-10288s	AB_521594	Goat	1:400	Tris
Anti-retinoic acid-binding protein 1 (CRABP1)	Cell Signaling Technology, Inc, 13163	AB_2750569	Rabbit	1:500	Tris
Anti- alpha-Smooth Muscle Actin (alpha-SMA)	Novus Biologicals, NB300-978	AB_2273628	Goat	1:200	Tris
Anti-SRY Box Transcription Factor 9 (SOX9)	Abcam, ab185230	AB_2715497	Rabbit	1:1000	None
Anti-macrophage mannose receptor (MMR) (CD206)	R&D Systems, AF2535	AB_2063012	Goat	1:500	Tris

226

Secondary Antibodies				
Antibody	**Company, Cat#**	**RRID**	**Host species**	**Dilution**
Alexafluor 594 anti-Rabbit	Thermo Fisher Scientific, A21207	AB_141637	Donkey	1:400
Alexafluor 647 anti-goat	Thermo Fisher Scientific, A21447	AB_2535864	Donkey	1:400
Alexafluor 647 anti-rat	Thermo Fisher Scientific, A21247	AB_141778	Goat	1:400

227

228 **Western Blotting.** Protein extraction and quantification was performed as indicated
229 (dx.doi.org/10.17504/protocols.io.rm7vzkx12vx1/v1). Western blotting was performed as
230 indicated (dx.doi.org/10.17504/protocols.io.kqdg3qxz1v25/v1).
231
232 **Imaging and Cell Quantification.** Fluorescent images were collected using Cells Sens from
233 Olympus in Olympus inverted microscope (Olympus America Inc). Whole tissue sections were
234 captured in 20X and stitched automatically. Cell counting was manually performed in defined

areas of the images separately in each channel using ImageJ. Percentages of positive cells were calculated by quantifying nuclei (Hoechst 33342) using the threshold tool in ImageJ.

Statistics. Statistical analyses were performed using JMP (version Pro 15.0, SAS Institute Inc) and SPSS (version 28.0, IBM) where alpha was set at 0.05 for all statistical analyses. Graphs were made in excel and JMP. To analyze our pulse chase data across species, we performed Two-way ANOVAs with either EdU+, BrdU+ or double positive cells (dependent variable), and days post injury (independent variable) followed by Tukey HSD multiple comparisons to test for differences in positive cells as a function of time (Supplementary table S2).

To analyze proliferation during regeneration in *Acomys*, we used a linear mixed model to assess differences in percentage of positive cells between three positions (A, B, C) over time (D5-D30) (Supplementary table S3). Likelihood ratio testing and Akaike Information Criterion (AIC) were used to select an appropriate covariance structure. A Kenward-Roger adjustment was used to correct for negative bias in the 170 standard errors and degrees of freedom calculations induced by the small sample size. Relevant pairwise comparisons were performed and controlled for multiple comparisons using Fisher's Least Significant Differences (LSD). Mixed modeling analysis was performed using SAS 9.4 (SAS Institute, Inc.; Cary, NC, USA).

Single-cell analysis. scRNA-seq data used in this study were download and available through the Gene Expression Omnibus (GEO) (RRID:SCR_005012) under the accession number GSE182141. The raw fastqs were processed through the CellRanger pipeline v8.0.1 (RRID:SCR_017344) using 10X Genomics' mm10-2020-A reference genome or a custom annotated *Acomys dimidiatus* genome (GCA_907164435.1 (mAcoDim1_REL_1905), with the 'include introns' set to true to obtain gene expression matrices.

Background reads were removed using decontX from the celda package using the filtered barcodes as the cells to keep and the remaining cells in the raw barcode matrix as the background (Campbell et al., 2024). Doublets were minimized using DoubletFinder (RRID:SCR_018771) (McGinnis et al., 2019). The R v4.4 (RRID:SCR_001905) library Seurat v5.1 (RRID:SCR_016341) (Hao et al., 2021; Hao et al., 2024)) was used for cell type clustering and marker gene identification. Cells expressing >500 genes were retained for downstream analysis. Each sample was normalized SCTransform v2 (RRID:SCR_022146), using the glmGamPoi

266 method and the number of RNA molecules per cell were regressed out. Samples were integrated
267 with common anchor genes using the CCA method to minimize sample to sample variation. Cell
268 clusters were determined by the Louvain algorithm using a resolution of 0.3. UMAP dimension
269 reduction was done using the first thirty principal components. Marker genes for each cell type
270 were calculated using the Wilcoxon Rank Sum test returning only genes that are present in a
271 minimum of 25% of the analyzed cluster. Cross species markers were done as above in cell types
272 of interest, but the pct.2 score was filtered to be > 0 to eliminate uniquely annotated genes from
273 dominating the lists. Volcano plots were created with the Enhanced Volcano (Blighe et al., 2024)
274 R library using the avg_log2FC and p_val_adj values as inputs.

275 Gene ontology (GO) analyses were performed in the Enrichr platform
276 (https://maayanlab.cloud/Enrichr/). Only differentially expressed genes with a two-fold change
277 were included in the analysis of GO Biological Process.

278

279 **RESULTS**

280

281 ***Vertebrate stromal cells rapidly re-enter the cell cycle in response to injury***

282 Complex tissue regeneration in vertebrates requires proliferation to expand cell
283 populations at the injury site which then undergo expansion and differentiation. Notably, few
284 papers using salamanders or fish to study regeneration have indicated whether stromal cells are
285 proliferating during normal homeostasis. To explore proliferation in uninjured tissue, we used
286 EdU to label cells in S-phase in two highly regenerative amniotes (*Danio rerio* - zebrafish,
287 *Ambystoma mexicanum* - axolotl), in an adult mammal with enhanced regenerative ability
288 (*Acomys dimidiatus* – spiny mouse) and in a poorly regenerating mammal (*Mus musculus* –
289 outbred ND4 laboratory mouse strain) (Fig. 1A). Examining the ear pinna (spiny mouse and lab
290 mouse), limb (axolotl) and caudal fin (zebrafish), we found cycling cells in the epidermis from
291 all four species prior to injury; a finding that was expected given the presence of slow cycling
292 stem cells in the epidermis (Fig. 1B). In uninjured *Danio* and *Ambystoma* tissue, we also found a
293 small percentage of cycling cells in the stroma (1% and 0.5% respectively) supporting previous
294 reports for these species (Fig. 1B-C) (K. Johnson et al., 2018; Simkin & Seifert, 2018). In
295 contrast, we found only one or two cycling stromal cells across entire tissue sections in *Acomys*

296 or *Mus* prior to tissue removal (Fig. 1B-C). These data support that stromal cell proliferation is
297 essentially non-existent prior to injury in mammals, at least in the ear and skin.
298 A longstanding hypothesis is that cells in non-regenerative vertebrates are refractory to
299 cell cycle re-entry and progression whereas cells in highly regenerative vertebrates easily re-
300 enter the cell cycle and proliferate to replace missing tissue (Pajcini et al., 2010; Simkin &
301 Seifert, 2018; Tanaka et al., 1997; Tanaka & Brockes, 1998). To test the capacity for cell cycle
302 re-entry in response to injury, we used a pulse chase strategy whereby we injected animals with
303 EdU, performed the specified injury, injected BrdU at either 15 or 63hrs post injury (hpi) and
304 then harvested tissue 9hrs later at 24 and 72 hpi (see Methods). We quantified stromal cells that
305 were EdU+, or BrdU+, or EdU+/BrdU+ (double positive) (Fig. 1B, D). 24 hpa spiny mice and
306 zebrafish showed the highest percentage of newly cycling cells in response to injury (BrdU+).
307 *Mus* cells also re-entered the cell cycle, albeit later at 72 hpa. Axolotl limb tissue, on the other
308 hand, exhibited very few singly BrdU+ cells but presented the highest number of double positive
309 cells (Fig. 1D). Importantly, our data demonstrate that stromal cells in *Acomys*, *Mus* and
310 zebrafish re-enter the cell cycle *de novo* in response to injury with a 48hr lag observed for *Mus*
311 cells.
312 To assess cell activation arising from the injury but independent of the local repair
313 response (i.e., systemic cell activation), we collected the contralateral ear pinna in *Mus* and
314 *Acomys*, the contralateral limb in axolotls, and the pelvic fin in zebrafish 24 hpa and 72 hpa after
315 tissue amputation. Using a pulse chase strategy as described above, we looked for cell cycle re-
316 entry in uninjured tissues at 24 hpa and 72 hpa. EdU+ cells were cycling prior to injury, BrdU+
317 cells were those activated systemically and EdU+/BrdU+ were those cycling prior to injury that
318 were activated systemically. Despite reports in lab mice of long-range cell activation in skeletal
319 muscle stem cells (Rodgers et al., 2014), in *Acomys* and *Mus*, we did not find a noticeable
320 response in the contralateral ear pinnae where the number of BrdU+ cells did not exceed 0.5% at
321 either time point (Fig. S1A-B). Similarly, in axolotl and zebrafish, the number of EdU+ cells at
322 24 hpa and 72 hpa was similar to the number of positive cells found in uninjured tissue at D0
323 (see above) (Fig. S1A-B). These data indicate that a systemic response to injury is negligible at
324 24 hpa and 72hpa in all four species.
325
326 ***Proliferating cells are maintained in a distal position relative to the wound site over time***

327 *Acomys* species can regenerate the ear pinna after tissue removal with a 4 mm (or larger)
328 ear hole punch whereas identical tissue excisions in wild or laboratory *Mus* resulted in scar tissue
329 formation (Seifert et al., 2012). Deeper examination revealed cycling cells at the injury site
330 during regeneration and failure to maintain a proliferative population during fibrotic healing
331 (Gawriluk et al., 2016). To more thoroughly understand the kinetics of proliferating cells during
332 regeneration and fibrotic repair, we again employed a pulse (EdU) chase (BrdU) scheme where
333 our pulse and chase were separated by a five-day window (see Methods). First, we analyzed
334 BrdU+ cells to estimate the proliferative rate from injury until D30 and then analyzed the spatial
335 distribution of cycling cells by quantifying cells adjacent to the injury (aka proximal) and at two
336 distal locations (i.e., closest to the new epidermis); distal dorsal and distal ventral (Fig. 2A-E). In
337 addition to the proliferative rate, we also quantified the total area of newly generated tissue from
338 D10-30 which supported continued addition of new tissue during regeneration (Fig. 2B). In
339 contrast, after a proliferative burst, no new fibrotic tissue was added in *Mus* ears after D10 (Fig.
340 2C).
341 Spatially analyzing BrdU+ cells from D10-30 during regeneration revealed that from D15
342 to D30, the number of cycling cells was significantly higher in the distal areas compared to the
343 proximal areas (injury site) while there was no difference between the distal-dorsal and distal-
344 ventral areas (Fig. 2D and Supplementary Table 1). The exception to this pattern was D20 when
345 the new tissue areas were small or flat and thus distal and proximal areas were close (Fig. 2D).
346 Importantly, the proliferative rate captured in the distal compartment remained >10% from D10-
347 30 which contributed to the steady production of new tissue while cell proliferation in the
348 proximal compartment decreased over time. (Fig. 2D). When we quantified BrdU+ cells in *Mus*
349 ears, we observed a narrow extension of new tissue (Fig. 2A). While we observed a proliferative
350 rate of >25% at D5 in *Mus,* the percent of BrdU+ cells precipitously declined from D10-30
351 which coincided with no increase in tissue area over this time period (Fig. 2C, E).
352 To assess the spatial distribution of cycling cells in the stromal compartment during the
353 proliferative phase of regeneration (D10-30), we first analyzed the epidermis as a simpler tissue
354 where stem cell localization and organization are well known. Basal stem cells are located in the
355 deeper layer of the epidermis and show symmetrical and asymmetrical cell division depending
356 on whether they produce progeny or more stem cells (Blanpain & Fuchs, 2006). Using our pulse-
357 chase scheme and based on localization, we observed stem, progenitor, and differentiating cells

358 in the epidermis (Fig. S2A-B). The stratum basale contained slow-cycling stem cells (strong
359 EdU+) and infrequently dividing stem cells (EdU+/BrdU+) while also indicating rapidly-cycling
360 progenitor cells (strong BrdU+/diluted EdU+), and recently-cycling progenitor cells (strong
361 BrdU+ Fig. S2A-B). In addition, we observed progenitor cells having acquired EdU that
362 migrated apically withdrawing from the cell cycle and undergoing differentiation as per the
363 absence of BrdU (Fig. S2B, yellow arrow). These cell behaviors demonstrated that our labeling
364 scheme could effectively capture predicted stem cell behavior in a tissue with known
365 proliferative properties.
366 Next we used this scheme to similarly characterize proliferative behavior in the stromal
367 compartment by quantifying cells that re-entered the cell cycle after injury but arrested within
368 five days (EdU+ only) possibly to differentiate or re-enter the cell cycle later (slow-cycling
369 progenitors), and cells that re-entered the cell cycle but maintained their proliferative state over
370 the same period (EdU+/BrdU+ and BrdU+ only) in both distal and proximal areas relative to the
371 wound site (Fig. 2F-I). We hypothesized that cell proliferation could either be clonal, with
372 multiple daughter cells near proliferative progenitors in rosettes or could expand from the wound
373 site. In the latter case, we predicted to capture progenitors cycling near the wound margin and
374 daughter cells building up the blastema distally. At D10, we found a random, stochastic pattern
375 of proliferation with a mixture of EdU+ cells, BrdU+ cells, and double-positive cells in distal and
376 proximal compartments, where the EdU+ cell population represented the biggest population
377 (>25%) (Fig. 2F-G). At D25, however, we were able to observe a pattern where rapid-cycling
378 (BrdU+) and infrequently-dividing (double positive) cells represented half of the proliferative
379 population (>9%) in the distal compartment with the other half (~8%) being represented by
380 potentially slow cycling progenitors (EdU+) (Fig. 2H-I). In comparison, the proximal area was
381 represented mostly by EdU+ cells (5%) that may have started differentiation and a very small
382 percentage of rapid-cycling and infrequently-dividing (1%) cells that could support expansion of
383 some differentiating cell types (Fig. 2H-I). Supporting this pattern, we observed differentiation
384 of new hair follicles and cartilage near the wound site. *In toto*, these results show that the
385 proliferative progenitor population is maintained in a distal position relative to the wound site.
386 Furthermore, our pulse chase labeling supports cell cycle progression and asynchronous cell
387 proliferation during regeneration in *Acomys*, whereas thymidine analog incorporation without
388 cell division was observed in *Mus*, suggesting an S-phase arrest after D10.

389

390 ***The proliferative population comprises diverse cell types in Acomys***

391 As noted earlier, cell proliferation is required during epimorphic regeneration to supply
392 cells for new tissue generation. Having shown that cell cycle progression and division occur
393 during ear pinna regeneration in spiny mice, we next began characterizing the cellular
394 composition of the proliferative population (PP). To determine cell state or identity among the
395 PP, we co-labeled with cell type specific markers and EdU (see Methods). As previously shown
396 in uninjured tissue, we did not find any mesenchymal cell type in a proliferative state. We,
397 therefore, characterized the distribution of macrophages (IBA1+), chondroblasts (SOX9+) and
398 two fibroblast subtypes (CRABP1+ or αSMA+) in comparison with *Mus* to identify any obvious
399 differences in presence and location in various uninjured tissue compartments (Fig. S3A-J). We
400 found relatively few CD206+ and IBA1+ macrophages in both species (Fig. S3A, B, F, G).
401 Similarly, αSMA+ cells were few and mostly marking pericytes (Fig. S3E, J). We observed two
402 populations of SOX9+ cells in both species: one associated with the perichondrium along the
403 elastic cartilage, and another associated with the sebaceous gland and hair follicle (Fig. S3C, H).
404 Interestingly, we observed a population of CRABP1+ fibroblasts scattered throughout the
405 papillary dermis in *Acomy*s while these cells were not detectable in uninjured *Mus* skin (Fig.
406 S3D, I).

407 We next examined these same cell types at D5 (Fig. 3A-J). First, we observed that
408 multiple cell types re-entered the cell cycle in both species. By counting all the EdU+ cells in a
409 counting frame and then quantifying double positive cells we estimated the fraction of cycling
410 cells represented by each cell type. Because inflammation peaks at D5 (Gawriluk et al., 2020),
411 we hypothesized that a large fraction of proliferating cells would be macrophages. Instead,
412 IBA1+ and CD206+ cells represented only 5.3% and 4.95% of the PP respectively in *Acomys*
413 and 5.3% and 0.96% in *Mus* (Fig 3A-D). In *Acomys*, the two fibroblast subtypes (CRABP1+ and
414 αSMA+ cells) represented ~14% and 18.65% respectively while chondroblasts (SOX9+ cells)
415 represented ~16% of the PP in *Acomys* (Fig. 3E, G, H). Surprisingly, although totally absent
416 prior to injury in *Mus*, an emergent CRABP1 population represented 28.9% of the PP at D5 (Fig.
417 3I). SOX9+ and αSMA+ cells represented 7.96%, and 33% of the PP in *Mus* (Fig. 3F, J).
418 Together, this data supports that various cell types re-enter the cell cycle during both
419 regeneration and fibrotic repair.

420 As described earlier, by day 20, only *Acomys* maintains their proliferative population
421 during regeneration whereas activated cells did not appear to maintain cell cycle progression or
422 appreciably divide during fibrotic repair. Co-staining with EdU, we confirmed all the cell types
423 mentioned above remained part of the PP at D20 in *Acomys* (Fig. 4A-C and Fig. S4A, B). Of
424 note, we observed that CRABP1+, αSMA+, and SOX9+ cells were segregated spatially
425 throughout the blastema (Fig. 4A-C, G, H and Fig. S5A). At D0, the CRABP1+ population
426 seemed restricted to the papillary dermis (Fig. S3D and Fig. S5A). However, this population
427 expanded to other regions deeper in the dermis at D5 (Fig. 3G and Fig. S5A) and occupied the
428 dorsal part of the blastema with another, smaller population in the ventral papillary zone at D20
429 (Fig. 4A-A', G, H and Fig. S5A). In contrast, the αSMA+ fibroblast population was absent at D0
430 (Fig. S3E and Fig. S5A) but was found after injury in a distal and central position where reticular
431 fibroblasts localize (Fig. 3H-H' and Fig. S5A). At D20, this population was comparatively much
432 smaller in size and largely non-overlapping with CRABP1+ cells, and located ventrodistally near
433 the wound epidermis (Fig. 4B-B', G, H and Fig. S5A). Interestingly, while the blastema expands
434 and both populations maintain cell cycle progression, the αSMA+ fibroblasts seem to maintain a
435 small population at the very distal tip of the blastema and ends up disappearing in proximal
436 tissue. While the CRABP1+ population seems much more abundant occupying more space over
437 time in the blastema at D25 and D30 (Fig. 4G and H). The SOX9+ population was present in the
438 cartilage before injury (Fig. S3C and Fig. S5A) and distributed in the middle of the blastema
439 perfectly aligned with the uninjured cartilage after injury (Fig. 4C and Fig. S5A). Finally, IBA1+
440 and CD206+ cells were spread evenly across the blastema (Fig. S4A-B and Fig. S5A). Assessing
441 the spatial segregation of these cell types in *Mus*, we noted a much different configuration of
442 these populations (Fig. 4D-F and Fig. S5B). We found that the CRABP1+ population in *Mus* was
443 absent at D0 (Fig. S3I and Fig. S5B) and then expanded throughout the injury zone at D5 (Fig. 3I
444 and Fig. S5B). However, this population became restricted to the very distal tip of the ear and the
445 staining was significantly fainter at D20 compared to cells we observed at D5 (Fig. 4D and Fig.
446 S5B). Although, the αSMA population was absent in *Mus* at D0 like in *Acomys* (Fig. S3E, J and
447 Fig. S5B), it became the dominant population in the distal part of the scar after injury (Fig. 4E
448 and Fig. S5B). We did observe some Sox9+ cells in the middle of the outgrowth (Fig. 4F and
449 Fig. S5B), and IBA1+ and CD206+ cells distributed widely throughout the scar tissue (Fig. S4C,
450 D and Fig. S5B).

451 These results show that the same cell types re-enter the cell cycle after injury in both
452 species, but only *Acomys* maintains cells in a proliferative state during regeneration.
453 Furthermore, we show a distinct spatial segregation of cell types in regeneration and scarring and
454 demonstrate that the CRABP1 population is present in *Acomys* before and after injury, while
455 there is only a transient expansion of this population in *Mus* immediately after injury. To further
456 support the expression pattern of CRABP1 observed in *Acomys* and *Mus*, we performed a
457 western blot and found high expression before and after injury in *Acomys* and little to no
458 expression in *Mus* before injury with an increase in expression at D10 and decrease at D20 (Fig.
459 S5C). Together, these data support that an expansive and persistent CRABP1+ population is
460 unique to regeneration.
461
462 ***Species-specific cell states separate scaring and regeneration phenotypes***
463 To support and extend our proliferation and cell studies, we interrogated a single-cell
464 RNA sequencing (scRNA-seq) dataset harvested from uninjured ear pinna (D0) and healing
465 tissue at D3, 5, 10 and 15 from *Acomys* and *Mus* (Simkin et al., 2024). Unbiased clustering of
466 batch corrected data for all time points (see Methods) revealed the same cell populations in both
467 species (Fig. S7). Next, we extracted the four main stromal cell populations, fibroblasts (cluster
468 18), chondroblasts (cluster 19), lymphatic endothelial cells (cluster 16) and vascular endothelial
469 cells (cluster 9), and generated a new UMAP (Fig. 5A). This re-clustering revealed eight
470 subpopulations among the four original stromal populations: two populations each of vascular
471 and lymphatic endothelial cells, three fibroblast subtypes, and a single chondroblast population
472 (Fig. 5B). To investigate markers from our immunohistochemical analysis, we plotted *Crabp1*,
473 *Acta2* (αSMA), and *Sox9* across cells on this UMAP (Fig. 5B). Interestingly, we found that
474 *Acta2* transcripts were strongly associated with one fibroblast subtype (cluster 7) while *Crabp1*
475 was totally excluded from this cluster (Fig. 5B-D). *Sox9* marked chondroblasts (cluster two) in
476 both species (Fig. 5E). Since we noticed cells expressing *Acta2* in clusters four and six in both
477 species, we plotted *CRABP1 and Acta2* together and found very few double positive cells in
478 *Acomys* (Fig. S8A). In contrast, fibroblast cluster six was mostly double-positive for *Crabp1* and
479 *Acta2* in *Mus* (Fig. S8B). In addition, fibroblast cluster four and lymphatic endothelial cluster
480 five were heavily enriched for *Acta2* in *Mus* (Fig. S8B). Together with our immunohistochemical
481 results, these data support a distinct fibroblast population that is *Acta2*+ in both species (cluster

482 7). However, they also support that a *Crabp1*+ fibroblast subtype exists in *Acomys* that does not
483 express *Acta2* whereas in *Mus*, *Crabp1* appears to mark only a transitional cell state to finally
484 express *Acta2*. Moreover, increased *Acta2* positivity among additional fibroblasts and lymphatic
485 endothelial cells in *Mus* support a bias in the mouse healing response towards fibrosis.
486 To further understand intrinsic differences between the fibroblast subpopulations in both
487 species, we ran differential gene expression (DGE) analysis comparing the three *Acomys*
488 fibroblast clusters against the three *Mus* clusters (Fig. 5F-K). This analysis revealed 1497 genes
489 (488 in *Acomys*, 1009 in *Mus*) differentially upregulated in cluster four, 1228 (510 in *Acomys*,
490 718 in *Mus*) in cluster six, and 743 (248 in *Acomys*, 495 in *Mus*) in cluster seven among both
491 species (Fig 5F, H, J). Gene ontology of each cluster separated by species revealed a clear
492 segregation in fibroblast responses to amputation (Supplementary Table S4). The three
493 fibroblasts clusters in *Mus* were associated with fibrotic pathways such as: cellular response to
494 Transforming Growth Factor Beta stimulus (GO:0071560), cellular response to hypoxia
495 (GO:0071456), and negative regulation of epithelial cell proliferation (GO:0050680), among
496 others (Fig 5G, I, K). In contrast, *Acomys* subpopulations were associated with telomere
497 maintenance and cell proliferation pathways. Clusters four and six, for example, were associated
498 with positive regulation of establishment of protein localization to telomere (GO:1904851),
499 positive regulation of telomerase RNA localization to Cajal Body (GO:1904874), and response
500 to Endoplasmic Reticulum Stress (ERS) (GO:0034976) (Fig. 5G, I). Interestingly, *Acta2* (marker
501 associated with myofibroblasts) expressing cluster seven was associated with regulation of fat
502 cell differentiation (GO:0045598), positive regulation of translation (GO:0045727) and
503 regulation of membrane protein ectodomain proteolysis (GO:0051043) (Fig 5K). Chondroblasts
504 (cluster two) also followed the same pattern with 2234 genes (786 in *Acomys*, 1448 in *Mus*)
505 differentially upregulated. *Acomys* chondroblasts upregulated genes associated with translation
506 (GO:0006412), response to hydrogen peroxide (GO:0042542) and gene expression
507 (GO:0010467), while *Mus* chondroblasts upregulated genes associated with cellular response to
508 Transforming Growth Factor Beta stimulus (GO:0071560) and regulation of Transforming
509 Growth Factor Beta Receptor signaling pathway (GO:0017015) (Fig. S9B). Of note, all four
510 clusters (two, four, six and seven) in *Acomys* highly upregulated *Zc3h10* and *Tssc4* (Fig. 5F, H, J
511 and fig. S9A). The first gene has been shown to boost mitochondrial function (Audano et al.,

512 2018), while the second gene promotes cell survival and proliferation in breast cancer tumors
513 (Chen et al., 2022).
514 Together, these data show that all four *Mus* subpopulations activate fibrosis-related
515 pathways, while the four subpopulations in *Acomys* are biased toward pathways associated with
516 cell proliferation and growth. Importantly, while the same markers may be able to identify
517 fibroblast subtypes in both species, the intrinsic ability of each subtype to respond to injury
518 differs.
519
520 ***CRABP1+ fibroblasts do not induce regeneration in neonatal Mus.***
521 Previous studies using very large wounds in lab mice observed hair follicle cells in the
522 center of the wound bed, an observation that has been attributed to the presence of *Crabp1+*
523 fibroblasts (the so-called WIHN model) (Jiang & Rinkevich, 2021; Phan et al., 2021b). Since we
524 did not observe CRABP1+ cells in uninjured *Mus* ear pinna tissue, but did observe them in
525 *Acomys* ear dermis prior to injury and during regeneration, we hypothesized these cells might
526 disappear during *Mus* ear development. To test this hypothesis, we assessed CRABP1 reactivity
527 in embryonic, neonatal, juvenile and adult ear tissue (Fig. 6A). In *Acomys,* we found CRABP1+
528 reactivity to cells across all stages (embryonic and neonatal) and into adulthood (8 months old)
529 (Fig. 6A). CRABP1 reactivity was strongest at embryonic stages but always restricted to the
530 developing dermis where it persisted into adulthood, mainly in the papillary dermis (Fig. 6A). In
531 contrast, we found that *Mus* fibroblasts started to lose CRABP1 expression around P20 and it
532 was totally absent from the ear pinna in three month old adults (Fig. 6A).
533 Based on these observations, we hypothesized that challenging *Mus* ear pinnae using our
534 regeneration assay in the presence of CRABP1+ fibroblasts might lead to enhanced ear hole
535 regeneration in *Mus*. Therefore, we performed a 4 mm ear punch in P20 animals and found that
536 neonatal ear holes produce tissue till D15 (Fig. 6B-C). Similarly, we performed 2 mm punches in
537 P23 animals and reported tissue growth till D20 (Fig. S10A-B), although we did not observe
538 regeneration. We went back and performed another assay in P15 *Mus* and collected tissue at D5
539 and D20. Although P15 uninjured tissue also has CRABP1+ fibroblasts, CRABP1 reactivity
540 after injury was similar to that observed in adult *Mus* with increased expression at D5 and then
541 disappearing by D20 (Fig 6D). Together, these data show the presence of a CRABP1+ fibroblast

542 population in neonatal *Mus* is not sufficient to promote a regenerative response and support an
543 intrinsic difference in the capacity for this population to respond to injury across species.
544
545
546 **DISCUSSION**
547 We previously reported that in response to an ear pinna injury, *Acomys* cells progress
548 through the cell cycle and maintain proliferation during regeneration. In response to an identical
549 injury in laboratory mouse strains (*Mus*), cell proliferation in the stromal compartment was
550 minimal, where cells initiated proliferation only to arrest shortly afterwards (Gawriluk et al.,
551 2016). Here, we conducted a comprehensive spatiotemporal analysis of cell cycle re-entry,
552 progression, and proliferation during regeneration and found cycling cells maintained a distal
553 position relative to the original injury, while proximal cells exited the cell cycle and
554 differentiated. Importantly, these data revealed finely controlled regulation of the cell cycle in
555 response to injury such that while the injury served as an activation trigger in both species, cells
556 in tissue destined to regenerate maintained cell cycle progression while those participating in
557 fibrotic repair arrested. Importantly, proliferation in *Acomys* did not lead to tissue overgrowth
558 demonstrating regulated shutdown of cell cycle progression. Examples of cell proliferation in
559 organ stroma where dedicated stem cell populations are not present are rarely observed except
560 for neoplasms where cell proliferation is uncontrolled and caused by the accumulation of genetic
561 mutations (Hanahan & Weinberg, 2011). Tightly controlled cell proliferation is a hallmark of
562 regenerating tissues, occurring in amputated zebrafish caudal fins (Nechiporuk & Keating, 2002;
563 Poleo et al., 2001) and newt limbs (Hays & Fischman, 1961; Wallace & Maden, 1976).
564 Although the evolutionary basis for the presence of regenerative ability among some
565 vertebrate clades remains controversial, indeterminate growth has been hypothesized as a
566 contributing factor because animals with determinate growth tend not to regenerate as adults
567 (Froehlich et al., 2013; Sebens, 1987). This longstanding hypothesis suggests that indeterminate
568 growers maintain populations of somatic stem or progenitor cells that behave like slow-cycling
569 stem cells to support growth. There are two arms to this hypothesis. The first is the presence of
570 cycling cells during normal homeostasis and growth lowers the barrier to cell cycle re-entry. The
571 second is that once cycling, cells do not activate tumor suppressor machinery during S-phase
572 progression to initiate cell cycle exit. These ideas stem from observations using newt myotubes

573 which easily re-enter the cell cycle in culture after serum stimulation in contrast to mouse
574 myotubes formed from C2C12 cells which are refractory to cell cycle re-entry after the same
575 treatment (Tanaka et al., 1997; Tanaka & Brockes, 1998). *Mus* myotubes can be forced to re-
576 enter through the cell cycle by deleting or inactivating tumor suppressors such us the
577 retinoblastoma protein (pRB) or $p16^{ink4a}$ (Gu et al., 1993; Schneider et al., 1994). The question
578 arises, do cycling cells in uninjured tissue contribute to regeneration?
579 To examine this question, we compared cell cycle re-entry and progression prior to and
580 after injury between determinate (*Acomys*, regeneration-competent; *Mus*, regeneration-
581 incompetent) and indeterminate growers (*Ambystoma* and *Danio* – regeneration-competent). In
582 line with previous observations (K. Johnson et al., 2018; Simkin & Seifert, 2018), we found a
583 small population of slow-cycling stromal cells present during homeostasis in indeterminate
584 growers while we failed to detect these cells in determinate growers. However, the cycling
585 population observed pre-injury in zebrafish scarcely contributed to blastema formation. Instead,
586 cells that re-entered the cell cycle in response to injury were the major contributors to
587 regeneration. This result supports a previous study in zebrafish where slow-cycling cells marked
588 for eight weeks before injury did not contribute to blastema formation (Nechiporuk & Keating,
589 2002). In our experiments, axolotls had the highest number of double positive cells after injury
590 suggesting that slow-cycling cells substantially contribute to the blastema. However, a relatively
591 long S-phase time (~53hrs) for axolotl cells (Wallace & Maden, 1976) may explain this result.
592 Importantly, our data show that cells in both *Acomys* and *Mus* re-enter the cell cycle in response
593 to injury independent of their regenerative ability. An open question is how cell cycle
594 progression is controlled for almost forty days and then downregulated so as not to create tissue
595 overgrowth. Considered *in toto*, our cross-species analysis rejects the notion that a determinate
596 growth mode prevents cell cycle re-entry and supports that the contribution of slow-cycling cells
597 to the blastema is minimal, at least in fish.
598 Another question we examined with our cross-species study was the extent to which
599 injury induced a systemic activation of cells distant from the injury site. Work in lab mice found
600 that acute muscle injury elicits a systemic response in which contralateral-located stem cells
601 (CSCs) re-enter the cell cycle and access a priming state named G_{Alert} (Rodgers et al., 2014). In
602 contrast to quiescent stem cells (QSCs), CSCs in mouse show an increased propensity to cycle,
603 although their numbers remain low in comparison with stem cells located at the injury site

604 (Rodgers et al., 2014). A similar systemic response was observed in axolotl limbs contralateral to
605 amputated limbs (Johnson et al., 2018). Using contralateral control tissue collected in our
606 experiments, we looked for primed cells *in vivo* following injury. In contrast to muscle stem cells
607 in *Mus*, we found a negligible stromal response in *Acomys* and *Mus* with less than 0.5% of
608 contralateral ear pinna cells responding to a systemic signal. This difference may be explained by
609 our methodology used to assess proliferation and by the specific cell types analyzed. While we
610 used immunofluorescence to quantify active or primed mesenchymal cells in tissue sections,
611 previous studies in mouse muscle used FACS sorted satellite stem cells to assess *in vivo* BrdU
612 incorporation. Supporting our observations in *Acomys* and *Mus*, we could not find a significant
613 response in contralateral axolotl limbs or zebrafish pelvic fins, at least in the first 72hrs after
614 injury. While these results are at odds with a single axolotl study, those data included epidermal
615 cells in their cell counts and later time points (Johnson et al., 2018). Together, our data do not
616 support significant cell cycle re-entry in uninjured contralateral tissue from the four species
617 analyzed.
618 Contemporary regeneration studies have revisited cell type contributions to the blastema
619 with many studies exploring lineage contributions using transgenics in regenerative models. The
620 general consensus is that the blastema particular to an injured tissue is formed from a
621 heterogeneous population of cells at the amputation plane (Seifert & Muneoka, 2018). Although
622 various stem cell reservoirs have been discovered in different mammalian tissues, except for the
623 digit tip, exploring cell type contributions during complex tissue regeneration in mammals has
624 been impossible. While we could not identify stem cells with our methods, our data support that
625 *Acomys* expands pre-existing cell types to participate in regeneration via cell proliferation. One
626 exception in our analysis were αSMA+ fibroblasts which appeared after injury but did not
627 maintain αSMA identity in newly differentiated tissue. Interestingly, our scRNA-seq data
628 indicated that an *Acta2* expressing population expresses genes related to the regulation of fat cell
629 differentiation suggesting that some myofibroblasts may differentiate into adipocytes in a
630 regenerative context. Similarly, αSMA+ myofibroblasts were shown to differentiate into
631 adipocytes when exposed to bone morphogenetic protein (BMP) triggered by neogenic hair
632 follicles in large skin wounds (Plikus et al., 2017). Further supporting our observations, recent
633 data from another *Acomys* ear pinna regeneration study reported that αSMA fibroblasts
634 disappear after wound closure with only ACTA2+ vascular smooth muscle cells remaining

635 (Brewer et al., 2021). In addition, we observed high expression of TGFβ pathway components in
636 *Mus*, but not *Acomys* fibroblasts. Taken with the previously observed insensitivity of *Acomys*
637 fibroblasts to TGFβ induced myofibroblast differentiation (Brewer et al., 2021), *Acomys* appears
638 to support reduced myofibroblast activation. While these data suggest a possible differentiation
639 trajectory for myofibroblasts, the exact dynamics of αSMA+ cells await further study in a
640 regenerative context.

641 In contrast to their role during regeneration, the role of myofibroblasts during fibrotic
642 skin repair is well known (rev. in Plikus et al., 2021). Previous studies in skin have described
643 first wound responders as a large proportion of reticular fibroblasts including αSMA fibroblasts
644 (Driskell et al., 2013) which rapidly seal the wound area promoting scaring and inhibiting hair
645 follicle formation (Correa-Gallegos et al., 2019). These data support our observations in *Mus*
646 where αSMA+ fibroblasts are the main cell population in newly generated scar tissue. Together,
647 these data show that αSMA fibroblasts are dominant in scaring but seem to be transient in
648 regeneration.

649 CRABP1+ papillary fibroblasts abundantly participate in the regeneration of neonatal
650 skin and deer antler velvet and thus we were interested to interrogate their behavior in our ear
651 pinna assay (Phan et al., 2021b; Sinha et al., 2022). In contrast to the ephemeral nature of the
652 αSMA+ population in *Acomys*, we observed a stark difference in CRABP1+ cells during
653 regeneration and fibrotic repair. While we were unable to detect CRABP1+ cells prior to injury
654 in *Mus*, these cells appeared at D5 as a subset of cycling cells only to disappear by D20. In
655 *Acomys*, however, we detected CRABP1+ cells prior to injury and this population expanded to
656 participate in blastema formation. CRABP1 has been found in a variety of regeneration contexts.
657 For instance, this protein is expressed in *Mus* papillary fibroblasts that expand in large,
658 somewhat regenerative wounds (Guerrero-Juarez et al., 2019). Other examples are the
659 regenerating wounds in newborn (P2) mice that have a higher proportion of CRABP1+
660 fibroblasts (Phan et al., 2021a) and the velvet skin on deer antlers which have regeneration-
661 primed fibroblasts expressing genes putatively associated with a regenerative phenotype (e.g.,
662 *CRABP1, RUNX1,* and *PRSS35*) (Sinha et al., 2022).

663 Rather than the presence or lack of a specific cell type, our scRNA-seq data suggests that
664 it may also be one of cell state. Although all four stromal subclusters express some of the same
665 markers in *Acomys* and *Mus*, our DGE and GO analyses revealed that the four *Mus* subclusters

666 express biological processes related to fibrosis. In contrast, all four subclusters in *Acomys* seem
667 to use biological processes related with cell proliferation; high transcription and telomere
668 maintenance and genes that boost mitochondrial function and cell survival. Specifically, a
669 subpopulation in both species that highly expressed *Acta2* exhibited divergent transcriptomic
670 responses. Future studies are necessary to address whether *Acomys* αSMA+ cells transiently
671 become myofibroblast-like only to later differentiate into adipocytes as suggested by our GO
672 analysis. Our finding that two subpopulations expressed high telomerase and endoplasmic
673 reticulum stress (ERS) related activity supported the persistence of proliferation in these cells.
674 Telomerase activity is low in most non-proliferating somatic cells in humans and mice, while
675 high activity has been reported in highly proliferating immortal and cancer cells (Kim et al.,
676 1994; Sha & Bacchetti, 1997). Moreover, inhibition of telomerase results in death of tumor cells
677 *in vitro* and *in vivo* showing the importance of this enzyme for tumor growth (Hahn et al., 1999).
678 Similarly, various ERS responses have been shown to promote cell proliferation and survival in
679 various types of cancer (Zhang et al., 2024). These data suggest that *Acomys* can access and use
680 pathways other adult mammals do not outside of tumorigenesis.
681 As a functional test of cell type versus cell state as a driver of regeneration, we assessed
682 the role of CRABP1+ fibroblasts after injury in neonatal mice before this population disappears.
683 Previous studies have shown that papillary CRABP1+ fibroblasts are enriched in regenerative
684 neonatal human and mouse skin but are lost early during postnatal development (Mine et al.,
685 2008; Sinha et al., 2022). Examining neonatal and early postnatal stages, we found CRABP1+
686 fibroblasts in the *Mus* ear pinna which persisted until approximately P20. Using our ear punch
687 assay, we did not find a significant improvement in ear hole closure or evidence of regeneration
688 in animals injured at P15 or P20. These results support that the presence of a cell population
689 alone is less important that the ability for cells to acquire a specific cell state needed to facilitate
690 regeneration. A recent examination of regeneration and scarring phenotypes across eleven murid
691 rodents, underscored the binary nature of a regenerative phenotype in that species appear to
692 either completely regenerate or not (i.e., no partial regeneration) (REF). This supports that
693 complex tissue regeneration requires multiple features across stereotypical healing processes
694 such as intrinsic cell cycle licensing (Gawriluk et al., 2016; Tomasso et al., 2023), goldilocks
695 regulation of reactive oxygen species (ROS) (Saxena et al., 2019) and a regenerative skewed
696 immune cell response (Gawriluk et al., 2020; Simkin et al., 2017, 2024). Future work

investigating specific cell states across more regenerative and non-regenerative mammals will undoubtably shed light on a blueprint for complex tissue regeneration in mammals.

ACKNOWLEDGEMENTS

We would like to thank Josh Sarli, Brennan Riddell and Ava Musarra for animal husbandry. We thank all members of the Seifert lab for helpful discussions in developing the manuscript and Brennan Riddle for helping to create the GO graphs. This research was funded in part by grants from the NIH (R01AR070313) and Aligning Science Across Parkinson's (ASAP-020495) through the Michael J. Fox Foundation for Parkinson's Research (MJFF) to AWS. For the purpose of open access, the author has applied a CC BY public copyright license to all Author Accepted Manuscripts arising from this submission.

AUTHOR CONTRIBUTIONS

EOR, RA, and AWS designed research. EOR, MA and RA performed research. EOR, MA and AWS analyzed data. EOR and AWS wrote the paper, and all authors commented on and edited the paper.

COMPETING INTERESTS

The authors declare no competing interests.

AVAILABILITY STATEMENT

The data, code, protocols, and key lab materials used and generated in this study are listed in a Key Resource Table alongside their persistent identifiers (Supplementary Tables).

REFERENCES

Audano, M., Pedretti, S., Cermenati, G., Brioschi, E., Diaferia, G. R., Ghisletti, S., Cuomo, A., Bonaldi, T., Salerno, F., Mora, M., Grigore, L., Garlaschelli, K., Baragetti, A., Bonacina, F., Catapano, A. L., Norata, G. D., Crestani, M., Caruso, D., Saez, E., … Mitro, N. (2018). Zc3h10 is a novel mitochondrial regulator. *EMBO Reports*, *19*(4). https://doi.org/10.15252/embr.201745531

Billingham, R. E., Mangold, R., & Silvers, W. K. (1959). THE NEOGENESIS OF SKIN IN THE ANTLERS OF DEER*. *Annals of the New York Academy of Sciences*, *83*(3), 491–498. https://doi.org/10.1111/J.1749-6632.1960.TB40922.X

Blanpain, C., & Fuchs, E. (2006). *Epidermal Stem Cells of the Skin*.

Blighe K, Rana S, Lewis M (2024). *EnhancedVolcano: Publication-ready volcano plots with enhanced colouring and labeling*. R package version 1.24.0, https://github.com/kevinblighe/EnhancedVolcano.

Borgens, R. B. (1982). Mice Regrow the Tips of Their Foretoes. *Science*, *217*(4561), 747–750. https://doi.org/10.1126/SCIENCE.7100922

Brewer, C. M., Nelson, B. R., Wakenight, P., Collins, S. J., Okamura, D. M., Dong, X. R., Mahoney, W. M., McKenna, A., Shendure, J., Timms, A., Millen, K. J., & Majesky, M. W. (2021). Adaptations in Hippo-Yap signaling and myofibroblast fate underlie scar-free ear appendage wound healing in spiny mice. *Developmental Cell*, *56*(19), 2722–2740. https://doi.org/10.1016/j.devcel.2021.09.008

Carlson, B. M. (2005). Some principles of regeneration in mammalian systems. *Anatomical Record. Part B, New Anatomist*, *287*(1), 4–13. https://doi.org/10.1002/AR.B.20079

Chen, Y., Zhang, Z., Henson, E. S., Cuddihy, A., Haigh, K., Wang, R., Haigh, J. J., & Gibson, S. B. (2022). Autophagy inhibition by TSSC4 (tumor suppressing subtransferable candidate 4) contributes to sustainable cancer cell growth. *Autophagy*, *18*(6), 1274–1296. https://doi.org/10.1080/15548627.2021.1973338

Cheung, T. H., & Rando, T. A. (2013). Molecular regulation of stem cell quiescence. In *Nature Reviews Molecular Cell Biology* (Vol. 14, Issue 6, pp. 329–340). https://doi.org/10.1038/nrm3591

Correa-Gallegos, D., Jiang, D., Christ, S., Ramesh, P., Ye, H., Wannemacher, J., Kalgudde Gopal, S., Yu, Q., Aichler, M., Walch, A., Mirastschijski, U., Volz, T., & Rinkevich, Y. (2019). Patch repair of deep wounds by mobilized fascia. *Nature*, *576*(7786), 287–292. https://doi.org/10.1038/s41586-019-1794-y

Driskell, R. R., Lichtenberger, B. M., Hoste, E., Kretzschmar, K., Simons, B. D., Charalambous, M., Ferron, S. R., Herault, Y., Pavlovic, G., Ferguson-Smith, A. C., & Watt, F. M. (2013). Distinct fibroblast lineages determine dermal architecture in skin development and repair. *Nature*, *504*(7479), 277–281. https://doi.org/10.1038/nature12783

Echeverri, K., Clarke, J. D. W., & Tanaka, E. M. (2001). In vivo imaging indicates muscle fiber dedifferentiation is a major contributor to the regenerating tail blastema. *Developmental Biology*, *236*(1), 151–164. https://doi.org/10.1006/dbio.2001.0312

Froehlich, J. M., Fowler, Z. G., Galt, N. J., Smith, D. L., & Biga, P. R. (2013). Sarcopenia and piscines: The case for indeterminate-growing fish as unique genetic model organisms in aging

764 and longevity research. *Frontiers in Genetics*, *4*(AUG).
765 https://doi.org/10.3389/fgene.2013.00159

766 Gawriluk, T. R., Simkin, J., Hacker, C. K., Kimani, J. M., Kiama, S. G., Ezenwa, V. O., & Seifert,
767 A. W. (2020). Complex Tissue Regeneration in Mammals Is Associated With Reduced
768 Inflammatory Cytokines and an Influx of T Cells. *Frontiers in Immunology*, *11*.
769 https://doi.org/10.3389/FIMMU.2020.01695/FULL

770 Gawriluk, T. R., Simkin, J., Thompson, K. L., Biswas, S. K., Clare-Salzler, Z., Kimani, J. M.,
771 Kiama, S. G., Smith, J. J., Ezenwa, V. O., & Seifert, A. W. (2016). Comparative analysis of
772 ear-hole closure identifies epimorphic regeneration as a discrete trait in mammals. *Nature*
773 *Communications*, *7*. https://doi.org/10.1038/ncomms11164

774 Gerber, T., Murawala, P., Knapp, D., Masselink, W., Schuez, M., Hermann, S., Gac-Santel, M.,
775 Nowoshilow, S., Kageyama, J., Khattak, S., Currie, J. D., Camp, J. G., Tanaka, E. M., &
776 Treutlein, B. (2018). Single-cell analysis uncovers convergence of cell identities during
777 axolotl limb regeneration. *Science*, *362*(6413). https://doi.org/10.1126/science.aaq0681

778 Goss, R. J. (1980). Prospects for Regeneration in Man. In *SECTION I11 BASIC SCIENCE AND*
779 *PATHOLOGY*.

780 Goss, R. J., & Grimes, L. N. (1972). Tissue Interactions in the Regeneration of Rabbit Ear Holes.
781 In *AM. Zooi.or.isr* (Vol. 12). https://academic.oup.com/icb/article/12/1/151/2107413

782 Gu, W., Schneider, J. W., Condorelli, G., Kaushai, S., Yahdavi, V., & Nadai-Ginard, B. (1993).
783 Interaction of Myogenic Factors and the Retinoblastoma Protein Mediates Muscle Cell
784 Commitment and Differentiation. In *Cell* (Vol. 72).

785 Guerrero-Juarez, C. F., Dedhia, P. H., Jin, S., Ruiz-Vega, R., Ma, D., Liu, Y., Yamaga, K.,
786 Shestova, O., Gay, D. L., Yang, Z., Kessenbrock, K., Nie, Q., Pear, W. S., Cotsarelis, G., &
787 Plikus, M. V. (2019). Single-cell analysis reveals fibroblast heterogeneity and myeloid-
788 derived adipocyte progenitors in murine skin wounds. *Nature Communications*, *10*(1).
789 https://doi.org/10.1038/s41467-018-08247-x

790 HAHN, W. C., STEWART, S. A., BROOKS, M. W., YORK, S. G., EATON, E., KURACHI, A.,
791 BEIJERSBERGEN, R. L., KNOLL, J. H. M., MEYERSON, M., & WEINBERG, R. A.
792 (1999). Inhibition of telomerase limits the growth of human cancer cells. *Nature*.

793 Hanahan, D., & Weinberg, R. A. (2011). Hallmarks of cancer: The next generation. In *Cell* (Vol.
794 144, Issue 5, pp. 646–674). https://doi.org/10.1016/j.cell.2011.02.013

795 Hao, Y., Stuart, T., Kowalski, M. H., Choudhary, S., Hoffman, P., Hartman, A., Srivastava, A.,
796 Molla, G., Madad, S., Fernandez-Granda, C., & Satija, R. (2024). Dictionary learning for
797 integrative, multimodal and scalable single-cell analysis. *Nature Biotechnology*, *42*(2), 293–
798 304. https://doi.org/10.1038/s41587-023-01767-y

799 Hao Y, Hao S, Andersen-Nissen E, Mauck WM 3rd, Zheng S, Butler A, Lee MJ, Wilk AJ, Darby
800 C, Zager M, Hoffman P, Stoeckius M, Papalexi E, Mimitou EP, Jain J, Srivastava A, Stuart

801 T, Fleming LM, Yeung B, Rogers AJ, McElrath JM, Blish CA, Gottardo R, Smibert P, Satija
802 R. (2021). Integrated analysis of multimodal single-cell data. Cell. Jun 24;184(13):3573-
803 3587.e29. doi: 10.1016/j.cell.2021.04.048. Epub 2021 May 31. PMID: 34062119; PMCID:
804 PMC8238499.

805 Hays, E. D., & Fischman, D. A. (1961). Origin of the Blastema in Regenerating Limbs of the Newt
806 Triturus viridescens An Autoradiographic Study Using Tritiated Thymidine to Follow Cell
807 Proliferation and Migration'. In *DEVELOPMENTAL BIOLOGY* (Vol. 3).

808 Jiang, D., & Rinkevich, Y. (2021). Distinct fibroblasts in scars and regeneration. In *Current*
809 *Opinion in Genetics and Development* (Vol. 70, pp. 7–14). Elsevier Ltd.
810 https://doi.org/10.1016/j.gde.2021.04.005

811 Johnson, G. L., Masias, E. J., & Lehoczky, J. A. (2020). Cellular Heterogeneity and Lineage
812 Restriction during Mouse Digit Tip Regeneration at Single-Cell Resolution. *Developmental*
813 *Cell*, *52*(4), 525-540.e5. https://doi.org/10.1016/j.devcel.2020.01.026

814 Johnson, K., Bateman, J., DiTommaso, T., Wong, A. Y., & Whited, J. L. (2018). Systemic cell
815 cycle activation is induced following complex tissue injury in axolotl. *Developmental*
816 *Biology*, *433*(2), 461–472. https://doi.org/10.1016/j.ydbio.2017.07.010

817 Jopling, C., Sleep, E., Raya, M., Martí, M., Raya, A., & Belmonte, J. C. I. (2010). Zebrafish heart
818 regeneration occurs by cardiomyocyte dedifferentiation and proliferation. *Nature*, *464*(7288),
819 606–609. https://doi.org/10.1038/nature08899

820 Kim, Nam. W., Piatyszek, Miezyslaw. A., Prowse, Karen. R., Harley, Calvin. B., West, Michael.
821 D., Ho, Peter. L. C., Coviello, Gina. M., Wright, Woodring. E., Weinrich, Scott. L., & Shay,
822 Jerry. W. (1994). Specific association of human telomerase activity with immortal cells and
823 cancer. *Science*.

824 Lehoczky, J. A., Robert, B., & Tabin, C. J. (2011). Mouse digit tip regeneration is mediated by
825 fate-restricted progenitor cells. *Proceedings of the National Academy of Sciences of the*
826 *United States of America*, *108*(51), 20609–20614. https://doi.org/10.1073/pnas.1118017108

827 Leigh, N. D., Dunlap, G. S., Johnson, K., Mariano, R., Oshiro, R., Wong, A. Y., Bryant, D. M.,
828 Miller, B. M., Ratner, A., Chen, A., Ye, W. W., Haas, B. J., & Whited, J. L. (2018).
829 Transcriptomic landscape of the blastema niche in regenerating adult axolotl limbs at single-
830 cell resolution. *Nature Communications*, *9*(1). https://doi.org/10.1038/s41467-018-07604-0

831 Liu, L., Michowski, W., Kolodziejczyk, A., & Sicinski, P. (2019). The cell cycle in stem cell
832 proliferation, pluripotency and differentiation. In *Nature Cell Biology* (Vol. 21, Issue 9, pp.
833 1060–1067). Nature Publishing Group. https://doi.org/10.1038/s41556-019-0384-4

834 Maden, M., & Wallace, H. (1976). *How X-Rays inhibit Amphibian Limb Regeneration*.

835 Mine, S., Fortunel, N. O., Pageon, H., & Asselineau, D. (2008). Aging alters functionally human
836 dermal papillary fibroblasts but not reticular fibroblasts: A new view of skin morphogenesis
837 and aging. *PLoS ONE*, *3*(12). https://doi.org/10.1371/journal.pone.0004066

Morgan, T. H. (1901). *Regeneration /*. New York : http://hdl.handle.net/2027/mdp.39015001913774

Nechiporuk, A., & Keating, M. T. (2002). A proliferation gradient between proximal and msxb-expressing distal blastema directs zebrafish fin regeneration. *Development*.

Neeham, A. (1953). Regeneration and Wound-healing. *BioScience*, *3*(1), 16–16. https://doi.org/10.1093/AIBSBULLETIN/3.1.16-F

Orford, K. W., & Scadden, D. T. (2008). Deconstructing stem cell self-renewal: Genetic insights into cell-cycle regulation. In *Nature Reviews Genetics* (Vol. 9, Issue 2, pp. 115–128). https://doi.org/10.1038/nrg2269

Pajcini, K. V., Corbel, S. Y., Sage, J., Pomerantz, J. H., & Blau, H. M. (2010). Transient inactivation of Rb and ARF yields regenerative cells from postmitotic mammalian muscle. *Cell Stem Cell*, *7*(2), 198–213. https://doi.org/10.1016/j.stem.2010.05.022

Phan, Q. M., Sinha, S., Biernaskie, J., & Driskell, R. R. (2021a). Single-cell transcriptomic analysis of small and large wounds reveals the distinct spatial organization of regenerative fibroblasts. *Experimental Dermatology*, *30*(1), 92–101. https://doi.org/10.1111/exd.14244

Phan, Q. M., Sinha, S., Biernaskie, J., & Driskell, R. R. (2021b). Single-cell transcriptomic analysis of small and large wounds reveals the distinct spatial organization of regenerative fibroblasts. *Experimental Dermatology*, *30*(1), 92–101. https://doi.org/10.1111/exd.14244

Plikus, M. V, Guerrero-Juarez, C. F., Ito, M., Li, Y. R., Dedhia, P. H., Zheng, Y., Shao, M., Gay, D. L., Ramos, R., Hsi, T.-C., Oh, J. W., Wang, X., Ramirez, A., Konopelski, S. E., Elzein, A., Wang, A., Supapannachart, R. J., Lee, H.-L., Lim, C. H., … Cotsarelis, G. (2017). *Regeneration of fat cells from myofibroblasts during wound healing*. https://www.science.org

Plikus, M. V., Wang, X., Sinha, S., Forte, E., Thompson, S. M., Herzog, E. L., Driskell, R. R., Rosenthal, N., Biernaskie, J., & Horsley, V. (2021). Fibroblasts: Origins, definitions, and functions in health and disease. In *Cell* (Vol. 184, Issue 15, pp. 3852–3872). Elsevier B.V. https://doi.org/10.1016/j.cell.2021.06.024

Poleo, G., Brown, C. W., Laforest, L., & Akimenko, M. A. (2001). Cell proliferation and movement during early fin regeneration in zebrafish. In *Developmental Dynamics* (Vol. 221, Issue 4, pp. 380–390). https://doi.org/10.1002/dvdy.1152

Rinkevich, Y., Lindau, P., Ueno, H., Longaker, M. T., & Weissman, I. L. (2011). Germ-layer and lineage-restricted stem/progenitors regenerate the mouse digit tip. *Nature*, *476*(7361), 409–414. https://doi.org/10.1038/nature10346

Rodgers, J. T., King, K. Y., Brett, J. O., Cromie, M. J., Charville, G. W., Maguire, K. K., Brunson, C., Mastey, N., Liu, L., Tsai, C. R., Goodell, M. A., & Rando, T. A. (2014). MTORC1 controls the adaptive transition of quiescent stem cells from G 0 to GAlert. *Nature*, *510*(7505), 393–396. https://doi.org/10.1038/nature13255

874 Saxena, S., Vekaria, H., Sullivan, P. G., & Seifert, A. W. (2019). Connective tissue fibroblasts
875 from highly regenerative mammals are refractory to ROS-induced cellular senescence.
876 *Nature Communications*, *10*(1). https://doi.org/10.1038/s41467-019-12398-w

877 Schneider, J. W., Gu, W., Zhu, L., Mahdavi, V., & Nadal-Ginard, B. (1994). Reversal of Terminal
878 Differentiation Mediated by p107 in Rb-/- Muscle Cells. In *New Series* (Vol. 264, Issue
879 5164).

880 Sebens, K. P. (1987). The ecology of indeterminate growth in animals. *Ann. Rev. Ecol. Syst*.

881 Seifert, A. W., Kiama, S. G., Seifert, M. G., Goheen, J. R., Palmer, T. M., & Maden, M. (2012).
882 Skin shedding and tissue regeneration in African spiny mice (Acomys). *Nature*, *489*(7417),
883 561–565. https://doi.org/10.1038/nature11499

884 Seifert, A. W., & Muneoka, K. (2018). The blastema and epimorphic regeneration in mammals. In
885 *Developmental Biology* (Vol. 433, Issue 2, pp. 190–199). Elsevier Inc.
886 https://doi.org/10.1016/j.ydbio.2017.08.007

887 Sha, J. W., & Bacchetti, S. (1997). A Survey of Telomerase Activity in Human Cancer. In *Eur J*
888 *Cancer* (Vol. 33, Issue 5).

889 Simkin, J., Aloysius, A., Adam, M., Safaee, F., Donahue, R. R., Biswas, S., Lakhani, Z., Gensel,
890 J. C., Thybert, D., Potter, S., & Seifert, A. W. (2024). Tissue-resident macrophages
891 specifically express Lactotransferrin and Vegfc during ear pinna regeneration in spiny mice.
892 *Developmental Cell*, *59*(4), 496-516.e6. https://doi.org/10.1016/j.devcel.2023.12.017

893 Simkin, J., Gawriluk, T. R., Gensel, J. C., & Seifert, A. W. (2017). *Macrophages are necessary*
894 *for epimorphic regeneration in African spiny mice*. https://doi.org/10.7554/eLife.24623.001

895 Simkin, J., & Seifert, A. W. (2018). Concise Review: Translating Regenerative Biology into
896 Clinically Relevant Therapies: Are We on the Right Path? In *Stem Cells Translational*
897 *Medicine* (Vol. 7, Issue 2, pp. 220–231). John Wiley and Sons Ltd.
898 https://doi.org/10.1002/sctm.17-0213

899 Sinha, S., Sparks, H. D., Labit, E., Robbins, H. N., Gowing, K., Jaffer, A., Kutluberk, E., Arora,
900 R., Raredon, M. S. B., Cao, L., Swanson, S., Jiang, P., Hee, O., Pope, H., Workentine, M.,
901 Todkar, K., Sharma, N., Bharadia, S., Chockalingam, K., … Biernaskie, J. (2022). Fibroblast
902 inflammatory priming determines regenerative versus fibrotic skin repair in reindeer. *Cell*,
903 *185*(25), 4717-4736.e25. https://doi.org/10.1016/j.cell.2022.11.004

904 Storer, M. A., Mahmud, N., Karamboulas, K., Borrett, M. J., Yuzwa, S. A., Gont, A., Androschuk,
905 A., Sefton, M. V., Kaplan, D. R., & Miller, F. D. (2020). Acquisition of a Unique
906 Mesenchymal Precursor-like Blastema State Underlies Successful Adult Mammalian Digit
907 Tip Regeneration. *Developmental Cell*, *52*(4), 509-524.e9.
908 https://doi.org/10.1016/j.devcel.2019.12.004

Tanaka, E. M., & Brockes, J. P. (1998). A target of thrombin activation promotes cell cycle re-entry by urodele muscle cells. *Wound Repair and Regeneration*, *6*(4), S-371-S-381. https://doi.org/10.1046/J.1524-475X.1998.60413.X/FORMAT/PDF

Tanaka, E. M., Gann, A. A. F., Gates, P. B., & Brockes, J. P. (1997). Newt Myotubes Reenter the Cell Cycle by Phosphorylation of the Retinoblastoma Protein. In *The Journal of Cell Biology* (Vol. 136, Issue 1).

Tomasso, A., Koopmans, T., Lijnzaad, P., Bartscherer, K., & Seifert, A. W. (2023). *An ERK-dependent molecular switch antagonizes fibrosis and promotes regeneration in spiny mice (Acomys)*. https://www.science.org

Vorontsova, M. A., Liosner, L. D., Allen, P. M., & Billett, F. (1960). *Asexual propagation and regeneration*.

Wallace, H. (1981). *Vertebrate Limb Regeneration* (John Wiley & Sons, Ed.; First edition).

Wallace, H., & Maden, M. (1976). THE CELL CYCLE DURING AMPHIBIAN LIMB REGENERATION. In *J. CeUSci.zo*.

Wenemoser, D., & Reddien, P. W. (2010). Planarian regeneration involves distinct stem cell responses to wounds and tissue absence. *Developmental Biology*, *344*(2), 979–991. https://doi.org/10.1016/j.ydbio.2010.06.017

Zhang, W., Shi, Y., Oyang, L., Cui, S., Li, S., Li, J., Liu, L., Li, Y., Peng, M., Tan, S., Xia, L., Lin, J., Xu, X., Wu, N., Peng, Q., Tang, Y., Luo, X., Liao, Q., Jiang, X., & Zhou, Y. (2024). Endoplasmic reticulum stress—a key guardian in cancer. In *Cell Death Discovery* (Vol. 10, Issue 1). Springer Nature. https://doi.org/10.1038/s41420-024-02110-3

945 **FIGURES AND LEGENDS**

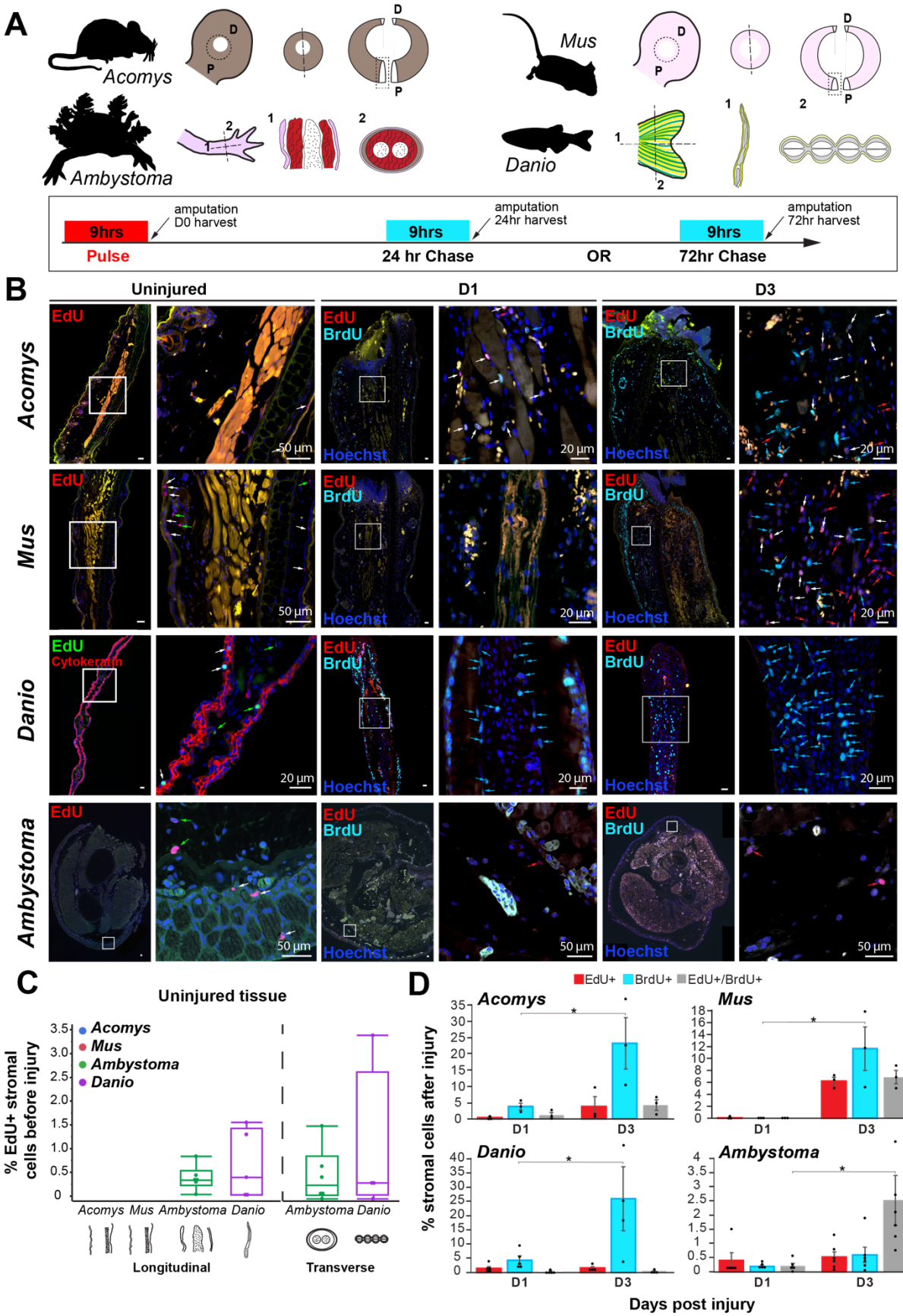
A
Acomys
Mus
Ambystoma
Danio
D
P
1
2
9hrs
amputation
D0 harvest
Pulse
24 hr Chase
OR
72hr Chase
amputation
24hr harvest
amputation
72hr harvest
B
Uninjured
D1
D3
Acomys
Mus
Danio
Ambystoma
EdU
BrdU
Hoechst
Cytokeratin
50 µm
20 µm
C
Uninjured tissue
% EdU+ stromal cells before injury
Acomys
Mus
Ambystoma
Danio
Longitudinal
Transverse
D
EdU+
BrdU+
EdU+/BrdU+
% stromal cells after injury
Days post injury
D1
D3

947 **Figure 1. Cell cycle re-entry before and after injury in *Acomys*, *Mus*, *Danio* and**
948 ***Ambystoma*.** A) Tissue section planes and EdU/BrdU pulse-chase scheme indicating injections
949 and harvest times; D = distal, P = proximal. B) Representative images of EdU+ and BrdU+ cells
950 in uninjured tissue (D0), D1 and D3. In uninjured tissue, white arrows = positive cells in the
951 epidermis and green arrows = positive cells in the stromal compartment. In injured tissue, red
952 arrows = EdU+ cells, light blue arrows = BrdU+ cells, and white arrows = double positive cells
953 (EdU+/BrdU+). C) EdU+ cell quantification as a percentage of the total number of cells in
954 uninjured tissue from all four species. Autofluorescent tissue, including red blood cells, stains in
955 multiple channels (yellow). D) EdU+, Brdu+ and EdU+/BrdU+ cell quantification as a
956 percentage of the total number of cells at D1 and D3 post-injury. Images represent n = 3
957 biological samples/time point in *Acomys* and *Mus*. See Methods for cell counting quantification.
958 In *Danio* (zebrafish), n = 9 at D0, n = 5 at D1 and n = 4 at D3. In *Ambystoma* (axolotl), n = 12 at
959 D0, n = 6 at D1, n = 6 at D3. (* $p<0.05$, ** $p<0.01$).

960

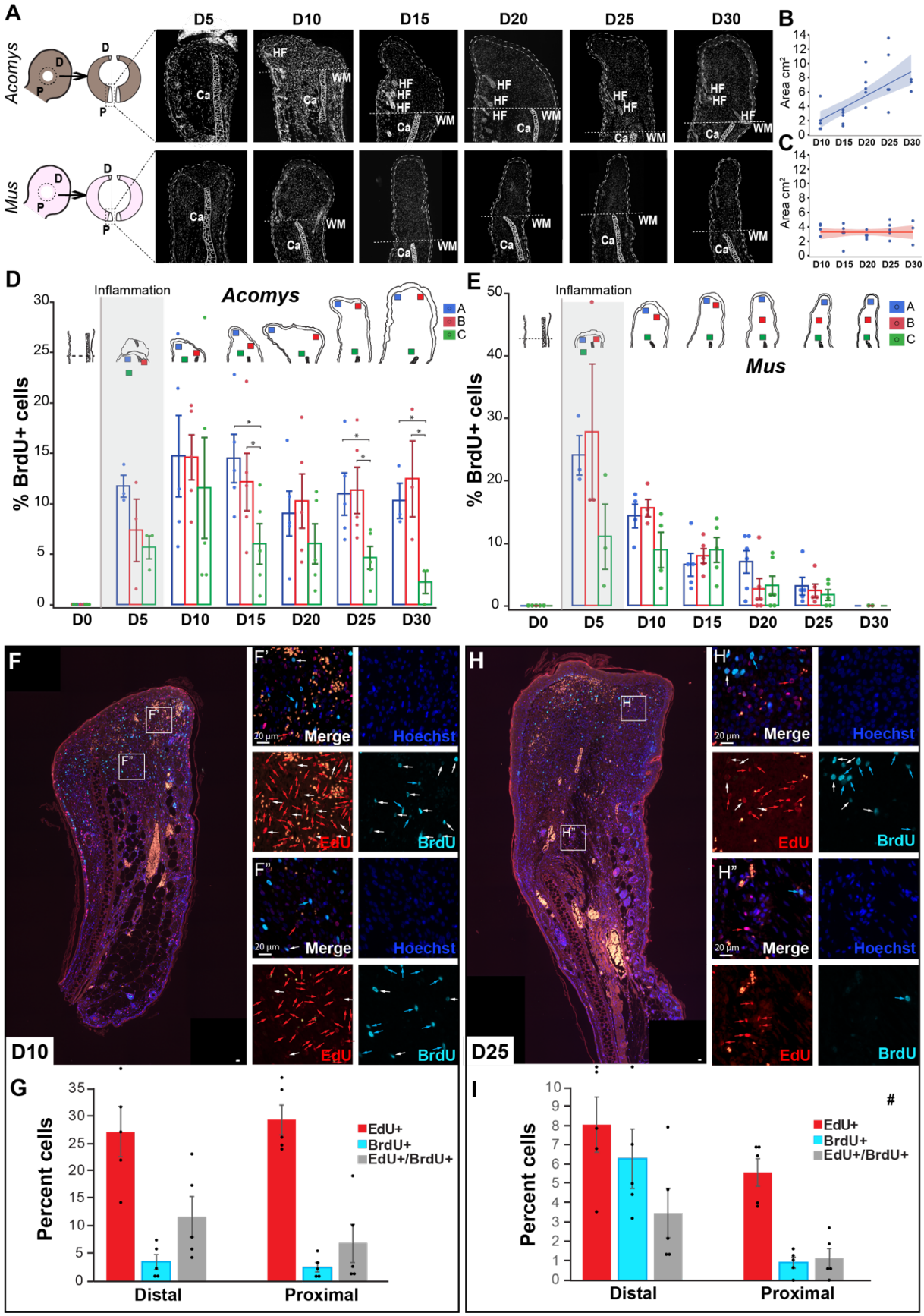
A
Acomys
Mus
D5
D10
D15
D20
D25
D30
Ca
HF
WM
B
C
Area cm²
D10 D15 D20 D25 D30
D
E
Inflammation
Acomys
Mus
% BrdU+ cells
A
B
C
D0 D5 D10 D15 D20 D25 D30
F
F'
F''
H
H'
H''
20 µm
Merge
Hoechst
EdU
BrdU
D10
D25
G
I
Percent cells
EdU+
BrdU+
EdU+/BrdU+
Distal
Proximal
#

961

962 **Figure 2. Spatiotemporal distribution of proliferating cells in *Acomys* and *Mus*.** A)
963 Representative images of blastema and scar tissue changes over time (D5-D30), Ca = cartilage,
964 WM = wound margin, HF = hair follicle. B-C) Blastema or scar tissue area in mm^2 from D10 to
965 D30 based on tissue sections. D-E) Quantification of BrdU+ cells as a percentage of the total
966 number of cells in three areas (A = blue, B = red, C = green) of the blastema in *Acomys* or the
967 scar in *Mus* from D5 to D30. F-H) Representative images of D10 (F) and D25 (H) blastema
968 tissue with EdU+, BrdU+ and double positive cells. Red arrows = EdU+ cells, light blue arrows
969 = BrdU+ cells, and white arrows = double positive cells (EdU+/BrdU+). G-I) Quantification of
970 EdU+, BrdU+ and EdU+/BrdU+ cells as a percentage of the total number of cells in distal and
971 proximal areas relative to the wound site at D10 (G) and D25 (I). n = 5 per time point per
972 species. (* $p<0.05$).

973

974

975

976

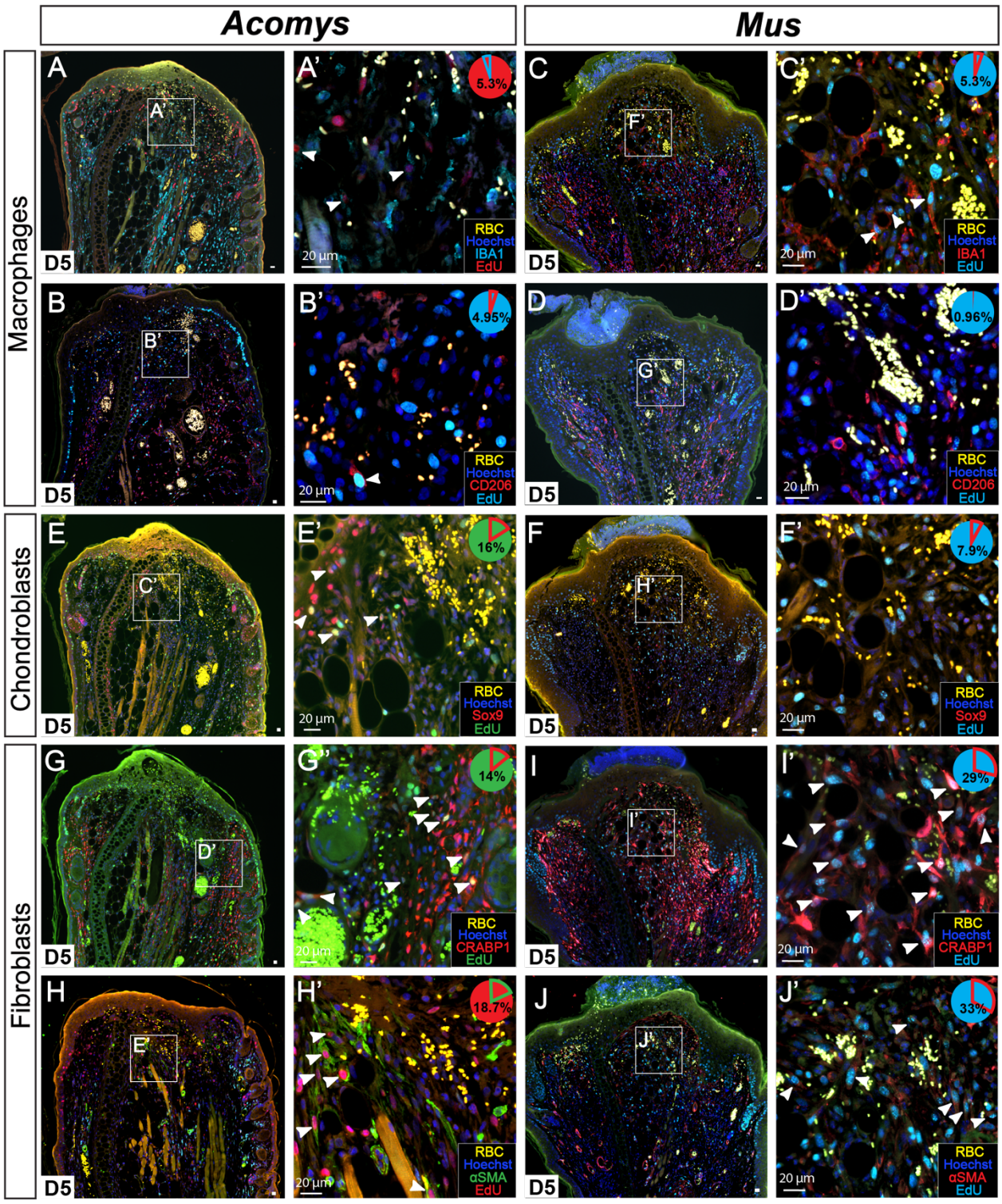

977

978 **Figure 3. S-phase quantification of fibroblasts, chondroblasts and macrophages after**
979 **injury at D5 in *Acomys* and *Mus*.** A-D) Cycling macrophages double labeled with IBA1 and
980 EdU in *Acomys* (A-A') and *Mus* (C-C') or with CD206 and EdU in *Acomys* (B-B') and *Mus* (D-

981 D'). E-F) Chondroblasts double labeled with Sox9 and EdU in *Acomys* (E-E') and *Mus* (F-F').
982 G-J) Fibroblasts double labeled with CRABP1 and EdU in *Acomys* (G-G') and *Mus* (I-I'). or
983 with αSMA and EdU in *Acomys* (H-H') and *Mus* (J-J'). White arrows indicate double positive
984 cells (EdU+/cell type marker). Pie charts indicate percentage double positive cells of the total
985 number of counted EdU+ cells. n = 5/species. RBC = red blood cells.

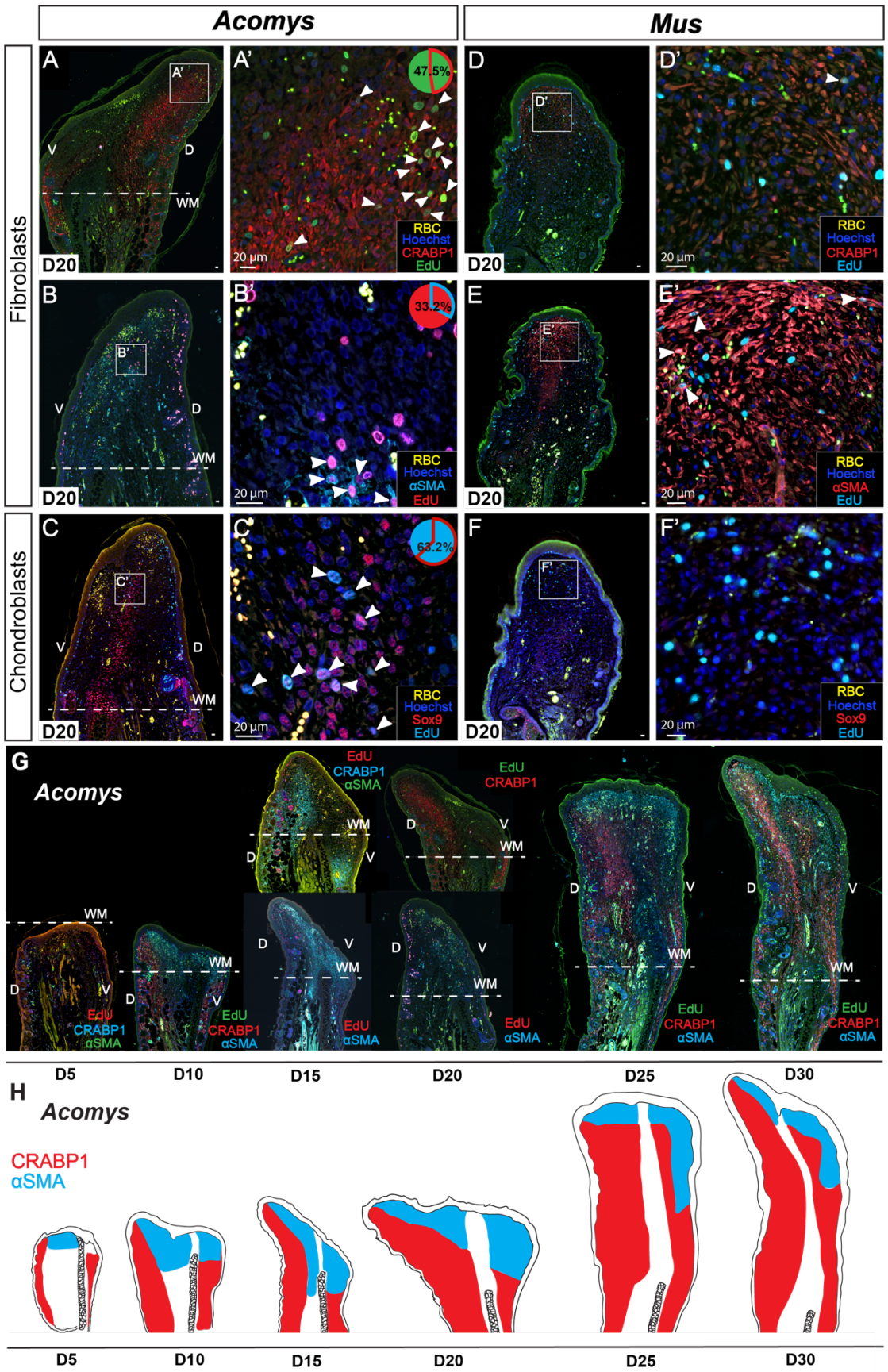
Acomys
Mus
Fibroblasts
Chondroblasts
A
A'
B
B'
C
C'
D
D'
E
E'
F
F'
V
D
WM
D20
47.5%
33.2%
63.2%
20 µm
RBC
Hoechst
CRABP1
αSMA
Sox9
EdU
G
Acomys
EdU
CRABP1
αSMA
H
Acomys
CRABP1
αSMA
D5
D10
D15
D20
D25
D30

986

987 **Figure 4. Spatial distribution of cell types within blastema or scar at D20.** A-C) CRABP1+
988 (A-A') or αSMA+ (B-B') fibroblasts, and Sox9+ chondroblasts (C-C') in *Acomys* at D20. D-F)
989 CRABP1+ (D-D') or αSMA+ (E-E') fibroblasts, and Sox9+ chondroblasts (F-F') in *Mus* at D20.
990 G) CRABP1 and αSMA double staining in *Acomys* over time (D5-D30). H) Cartoon showing
991 general distribution of CRABP1+ and αSMA+ fibroblasts in *Acomys.* White arrows indicate
992 double positive cells (EdU+/cell type marker). Pie charts indicate percentage double positive of
993 the total number of counted EdU+ cells. n = 5 per species. RBC = red blood cells.

994

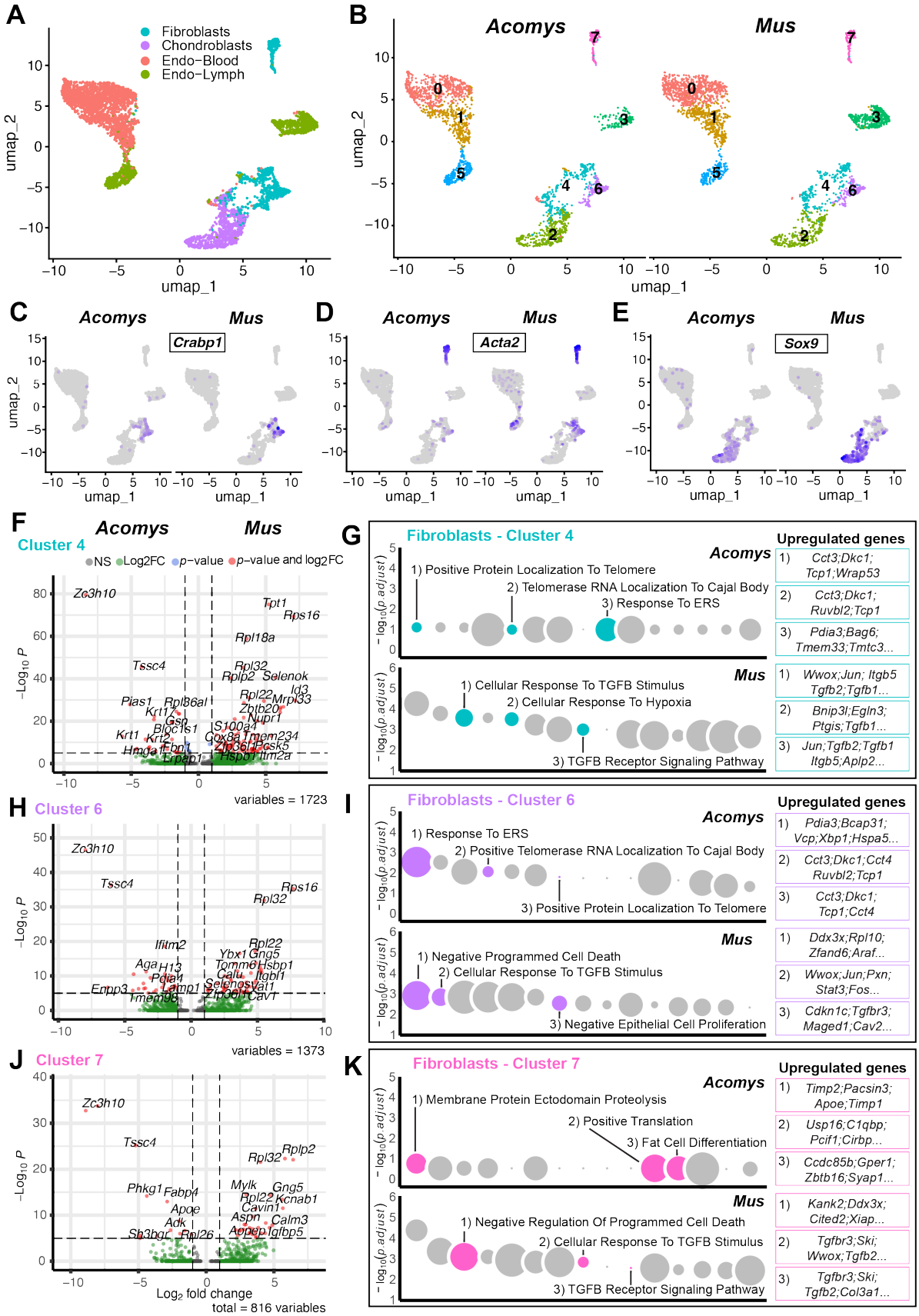
A
Fibroblasts
Chondroblasts
Endo−Blood
Endo−Lymph
umap_1
umap_2
B
Acomys
Mus
C
Crabp1
D
Acta2
E
Sox9
F
Cluster 4
NS
Log2FC
p−value
p−value and log2FC
variables = 1723
G
Fibroblasts - Cluster 4
1) Positive Protein Localization To Telomere
2) Telomerase RNA Localization To Cajal Body
3) Response To ERS
1) Cellular Response To TGFB Stimulus
2) Cellular Response To Hypoxia
3) TGFB Receptor Signaling Pathway
Upregulated genes
1) Cct3;Dkc1; Tcp1;Wrap53
2) Cct3;Dkc1; Ruvbl2;Tcp1
3) Pdia3;Bag6; Tmem33;Tmtc3...
1) Wwox;Jun; Itgb5 Tgfb2;Tgfb1...
2) Bnip3l;Egln3; Ptgis;Tgfb1...
3) Jun;Tgfb2;Tgfb1 Itgb5;Aplp2...
H
Cluster 6
variables = 1373
I
Fibroblasts - Cluster 6
1) Response To ERS
2) Positive Telomerase RNA Localization To Cajal Body
3) Positive Protein Localization To Telomere
1) Negative Programmed Cell Death
2) Cellular Response To TGFB Stimulus
3) Negative Epithelial Cell Proliferation
1) Pdia3;Bcap31; Vcp;Xbp1;Hspa5...
2) Cct3;Dkc1;Cct4 Ruvbl2;Tcp1
3) Cct3;Dkc1; Tcp1;Cct4
1) Ddx3x;Rpl10; Zfand6;Araf...
2) Wwox;Jun;Pxn; Stat3;Fos...
3) Cdkn1c;Tgfbr3; Maged1;Cav2...
J
Cluster 7
Log2 fold change
total = 816 variables
K
Fibroblasts - Cluster 7
1) Membrane Protein Ectodomain Proteolysis
2) Positive Translation
3) Fat Cell Differentiation
1) Negative Regulation Of Programmed Cell Death
2) Cellular Response To TGFB Stimulus
3) TGFB Receptor Signaling Pathway
1) Timp2;Pacsin3; Apoe;Timp1
2) Usp16;C1qbp; Pcif1;Cirbp...
3) Ccdc85b;Gper1; Zbtb16;Syap1...
1) Kank2;Ddx3x; Cited2;Xiap...
2) Tgfbr3;Ski; Wwox;Tgfb2...
3) Tgfbr3;Ski; Tgfb2;Col3a1...

996 **Figure 5. Single-cell analysis reveals different fibroblast cell states in *Acomys* and *Mus*.** Cell
997 suspensions collected from healing tissue preps representing D0, 3, 5, 10 and 15 were batch-
998 corrected and plotted together (Fig. S7) (see Methods). A) UMAP projection of stromal cell
999 types re-clustered from all cells (Fig. S7) from both species. B) UMAP projection of stromal
1000 subpopulations separated by species. Clusters represent subpopulations of major subtypes
1001 indicated in A. C-E) Feature plots for *Crabp1* (C), *Acta2* (D), and *Sox9* (E) separated by species.
1002 F, H, J) Volcano plots showing differentially upregulated genes between *Acomys* and *Mus* from
1003 clusters four (F), six (H), and seven (J) in B. Gene ontology Biological Process based on
1004 differentially upregulated genes between *Acomys* and *Mus* clusters four (G), six (I), and seven
1005 (K). Dot size represents the relative number of genes in each plot. Upregulated genes associated
1006 with each pathway are in color boxes. Refer to supplementary table S4 to see full list of genes.

1007

1008

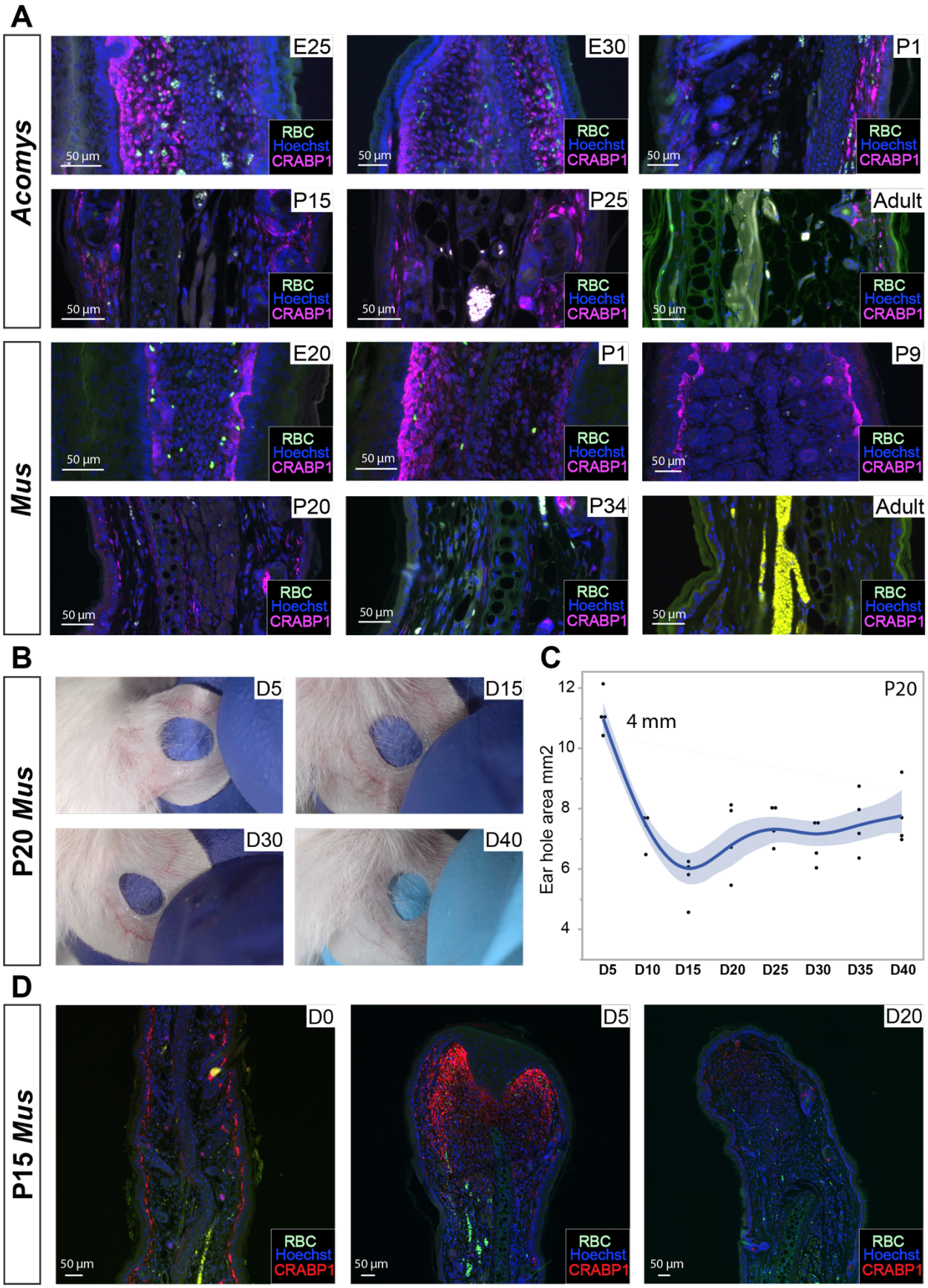
A
Acomys
E25
E30
P1
P15
P25
Adult
Mus
E20
P1
P9
P20
P34
Adult
RBC
Hoechst
CRABP1
50 µm
B
P20 Mus
D5
D15
D30
D40
C
P20
4 mm
Ear hole area mm2
12
10
8
6
4
D5
D10
D15
D20
D25
D30
D35
D40
D
P15 Mus
D0
D5
D20

1009

1010 **Figure 6. Tissue injury in neonatal mouse ears when CRABP1+ fibroblasts are present**
1011 **does not facilitate regeneration.** A) Immunostaining for CRABP1 in *Acomys* and *Mus*. Age in
1012 days indicated in upper right corner of each image. B) Images showing representative ear hole
1013 closure from P20 injured *Mus* after a 4 mm ear punch. C) Quantification of ear hole closure area
1014 from D5 to D40. D) CRABP1 staining in P15 *Mus* before and after injury. n = 3 per species per
1015 time point. Green channel shows autofluorescence including red blood cells (RBC).

1016

1017